

1 **Manuscript type: Article - Discovery**

2

3 **Conflicting evolutionary histories of the mitochondrial and nuclear genomes in New World *Myotis***

4 Roy N. Platt<sup>1</sup>, Brant C. Faircloth<sup>2</sup>, Kevin A.M. Sullivan<sup>1</sup>, Troy Kieran<sup>3</sup>, Travis C. Glenn<sup>3</sup>, Michael W.  
5 Vandewege<sup>1</sup>, Thomas E. Lee<sup>4</sup>, Robert J. Baker<sup>1</sup>, Richard D. Stevens<sup>5</sup>, David A. Ray<sup>1\*</sup>

6

7 <sup>1</sup> Department of Biological Sciences, Texas Tech University, Lubbock, USA

8 <sup>2</sup> Department of Biological Sciences and Museum of Natural Science, Louisiana State University, Baton  
9 Rouge, USA

10 <sup>3</sup> Environmental Health Science, University of Georgia, Athens, USA

11 <sup>4</sup> Department of Biology, Abilene Christian University, Abilene, USA

12 <sup>5</sup> Natural Resource Management, Texas Tech University, Lubbock, USA

13

14 \*Corresponding author: E-mail: david.4.ray@gmail.com

15

16 **Abstract**

17 The diversification of *Myotis* into more than 100 species in just a few million years is one of the  
18 most extensive mammalian radiations available for study. Efforts to understand relationships within  
19 *Myotis* have primarily utilized mitochondrial markers, and trees inferred from nuclear markers lacked  
20 resolution. Our current understanding of relationships within *Myotis* is therefore biased towards a set of  
21 phylogenetic markers that may not reflect the phylogenetic history of the nuclear genome. To resolve  
22 this, we sequenced the full mitochondrial genomes of 37 representative *Myotis*, primarily from the New  
23 World, in conjunction with targeted sequencing of 3,648 ultraconserved elements (UCEs). We inferred  
24 the phylogeny of *Myotis* and explored the effects of concatenation and summary phylogenetic methods,  
25 as well as combinations of markers based on informativeness or levels of missing data, on our  
26 phylogenetic results. Of the 295 phylogenies generated from the nuclear UCE data, all are significantly  
27 different from phylogenies inferred using mitochondrial genomes. Even within the nuclear genome  
28 quartet frequencies indicate that around half of all UCE loci conflict with the estimated species tree.  
29 Several factors can drive such conflict, including incomplete lineage sorting, introgressive hybridization,  
30 or even phylogenetic error. Despite the degree of discordance between nuclear UCE loci and the  
31 mitochondrial genome and among UCE loci themselves, the most common nuclear topology is  
32 recovered in one quarter of all analyses with strong nodal support. Based on these results, we re-

33 examine the evolutionary history of *Myotis* to better understand the phenomena driving their unique  
34 nuclear, mitochondrial, and biogeographic histories.

35

36 **Keywords**

37 incomplete lineage sorting, summary tree methods, concatenation, Vespertilionidae, phylogenomics,  
38 UCE, ultraconserved elements, reticulation

39

## 40 Introduction

41 The genus *Myotis* (Order Chiroptera, Family Vespertilionidae) contains more than 100 species  
42 that originated during the last 10-15 million years (Stadelmann, et al. 2007), making it one of the most  
43 successful, extant, mammalian species radiations. Members of *Myotis* are distributed worldwide,  
44 excluding polar regions, and generally share a similar ecological niche: aerial insectivory. *Myotis* species  
45 often exhibit little morphological differentiation and, as a result, the rate of cryptic speciation within the  
46 genus is thought to be high. For example, specimens identified as *M. nigricans* and *M. albescens* form  
47 multiple paraphyletic lineages distributed throughout the phylogeny of Neotropical *Myotis* (Larsen, et al.  
48 2012).

49 Confounding matters, the morphological variation that exists is often a poor indicator of  
50 species-level relationships. Early classifications of *Myotis* identified three major morphotypes (Findley  
51 1972); each were assumed to be monophyletic and were recognized at the subgeneric level (Simmons  
52 2005). Subsequent phylogenetic analyses of the mitochondrial cytochrome-b (*cytb*) gene recovered  
53 paraphyletic origins of the morphologically defined subgenera, suggesting convergent evolution in  
54 *Myotis* (Ruedi and Mayer 2001). These same analyses demonstrated that geography was a better  
55 predictor of phylogenetic relationship than morphology (Ruedi and Mayer 2001; Stadelmann, et al.  
56 2007). Generally, *Myotis* phylogenies from mitochondrial data contain a single bifurcation at the base of  
57 the tree that splits Old World from New World species. An additional bifurcation within New World  
58 species separates Nearctic (NA) from Neotropical (NT) species. The NA/NT bifurcation is not absolute,  
59 with at least five NA species located in the Neotropics and *vice versa*. The Old World/New World  
60 bifurcation is stricter, with only two Old World species, *M. brandtii* and *M. gracilis*, present in the New  
61 World clade.

62 The ability of mitochondrial markers to resolve a well-supported topology does not guarantee  
63 that the mitochondrial tree represents the species tree (for examples see Willis, et al. 2014; Li, et al.  
64 2016; Leavitt, et al. 2017). Despite containing 37 genes, the lack of recombination and uniparental  
65 inheritance of the mitochondrion means that it is transmitted as a single genetic unit. This makes  
66 mitochondria susceptible to evolutionary processes that may cause its history to diverge from the  
67 history of the species (Edwards and Bensch 2009). The most widely accepted phylogenies of *Myotis* rely  
68 heavily on mitochondrial data and even phylogenies containing nuclear data demonstrate an over  
69 reliance on mitochondrial markers for resolution. For example alignments of the nuclear *RAG2* and  
70 mitochondrial *cytb* contained 162 and 560 variable characters respectively (Stadelmann, et al. 2007).  
71 Phylogenetic analyses of *RAG2* in *Myotis* results in a tree primarily composed of polytomies

72 (Stadelmann, et al. 2007). Combining these two markers increases phylogenetic resolution, but the  
73 results are heavily influenced by larger numbers of mitochondrial characters, potentially masking signal  
74 from the nuclear marker (Stadelmann, et al. 2007; Larsen, et al. 2012; Ruedi, et al. 2013; Haynie, et al.  
75 2016).

76 It is difficult to draw major conclusions from studies limited in the number of characters (Ruedi  
77 and Mayer 2001; Stadelmann, et al. 2007; Larsen, et al. 2012; Ruedi, et al. 2013; Haynie, et al. 2016) or  
78 taxa (Platt, et al. 2015). Current data seem to indicate that nuclear and mitochondrial markers recover  
79 similar topologies. Platt et al. (2015) generated a phylogeny based entirely on nuclear data using 85,028  
80 shared transposable element insertions. Their results generally confirmed the mitochondrial  
81 phylogenies of *Myotis*, but only included seven taxa in their analysis. In order to fully resolve  
82 relationships and understand the *Myotis* radiation it is necessary to increase character and taxon  
83 sampling.

84 Recently, targeted sequencing methods have been developed that utilize baits to enrich and  
85 sequence ultraconserved elements (UCEs; Faircloth, et al. 2012), and this method has resolved a number  
86 of difficult phylogenetic problems (for examples see Crawford, et al. 2012; McCormack, et al. 2013;  
87 Green, et al. 2014; Faircloth, et al. 2015; McGee, et al. 2016). Generally speaking, the conserved “core”  
88 of UCE regions allows thousands of homologous loci to be enriched from divergent organismal genomes  
89 while the sequence that flanks the core UCE region contains a majority of phylogenetically informative  
90 sites – allowing researchers to collect a large number of phylogenetically informative, homologous loci  
91 from throughout the genome in a cost-effective and efficient manner. Broad sampling of the nuclear  
92 genome should help to resolve a phylogeny without an over reliance on mitochondrial loci. In addition,  
93 increasing the number of nuclear loci sampled from a handful of genes to thousands can recover  
94 accurate trees despite high levels of incomplete lineage sorting (Maddison and Knowles 2006)

95 Here, we used targeted sequencing of UCEs to collect ~1.4 Mbp from  $\geq 3,600$  nuclear loci in 37  
96 taxa, primarily representing New World *Myotis*. Combinations of the UCE data were analyzed using  
97 concatenation and tree summary methods to estimate the *Myotis* phylogeny. Analysis of the nuclear  
98 UCE data recovered 295 trees representing 175 distinct topologies. The nuclear topologies were  
99 compared to trees generated from full mitochondrial genomes to test for conflict between the two  
100 types of makers. Our results show that, despite the range of trees recovered from the nuclear data,  
101 nuclear and mitochondrial markers always depict conflicting phylogenies. Given that the nuclear and  
102 mitochondrial trees are distinct from one another it is necessary to reinvestigate conclusions made  
103 based solely on the mitochondrial phylogeny.

104

## 105 **Results**

106 We used targeted sequencing of UCEs to collect sequence data from 3,648 nuclear loci which we  
107 assembled into concatenated alignments as large as 1.37 Mb. In addition, we assembled mitochondrial  
108 genomes for most taxa. We then used the data to infer the phylogenetic history of New World *Myotis* in  
109 three phases: UCE and mitogenome assembly, initial phylogenetic analysis, extended phylogenetic  
110 analyses.

111 UCE and mitochondrial assembly and alignment – We averaged 3.29 million reads per sample  
112 after demultiplexing. These reads were assembled into an average of 5,778 contigs per sample (min =  
113 1,562 *M. martiniquensis*, max = 11,784 *M. nigricans* 3). Recovery of UCE loci varied across taxa. Of the  
114 5,500 loci in the Amniote probe set, we successfully recovered 3,898 UCE loci, 3,648 loci from five or  
115 more samples, 212 loci in all 37 samples (Table 2). On average, 3,332 UCE loci were recovered per  
116 sample, ranging from 1,106 (*M. martiniquensis*) 4,008 (*M. keaysi*). Repetitive sequences, identified via  
117 RepeatMasker searches, were minimal occupying less than 0.02% of sites across all UCE alignments.  
118 Sequence coverage of the mitochondrial genomes averaged 58x (range >1x - 297x). Mitochondrial  
119 genome assemblies varied in quality. Some were almost entirely complete while others were missing  
120 sections. We found three premature stop codons in mtDNA protein coding genes. Subsequent manual  
121 alignment and validation suggested that these regions were miscalled by MitoBim, and we corrected the  
122 errors prior to analysis.

123 Initial phylogenetic analyses – Initial analysis of the nuclear data used loci that were present in  
124 20 or more taxa. This resulted in an alignment of 1,144,471 bp from 2,890 nuclear loci containing 35,284  
125 parsimony informative characters. The 2,890 loci were split into 27 partitions as recommended by  
126 PartitionFinder (Lanfear, et al. 2012). Maximum likelihood and Bayesian analyses recovered the same  
127 topology and found similar support for most nodes (Figure 1A). Maximum likelihood analysis recovered  
128 100% support for 31 of 35 bipartitions, and 33 bipartitions were present in  $\geq 98\%$  bootstrap replicates.  
129 Nodes with the least support were still present in 86% - 88% of bootstrap replicates. After 50 bootstrap  
130 replicates the average weighted Robinson-Foulds distance between replicate sets was less than 0.23%  
131 (Pattengale, et al. 2009). Bayesian analysis recovered an identical topology, with the only difference  
132 being that all bipartitions were supported with a clade probability value of  $>0.99$ . Visual inspection of  
133 the parameter files in Tracer v1.6 showed good sampling with a likelihood score of  $-2.419 \times 10^{-6}$  and an  
134 effective sample size (ESS) of 637 for the likelihood parameter. All other parameters had effective

135 sample sizes greater than 500. The average standard deviation of split frequencies (ASDF) across all runs  
136 was less than 1% after 5,000 generations.

137 Thirty-seven mitochondrial protein coding, rRNA and tRNA genes were concatenated into single  
138 alignment of 15,520 bp containing 5,007 informative characters. Alignments for 30 samples were  $\geq 90\%$   
139 complete, and alignments for five samples were 68-84% complete. Only 21% and 50% of nucleotide  
140 positions were present in the *M. albescens*<sup>3</sup> (TK 61766) and *Myotis levis* alignments. Maximum likelihood  
141 and Bayesian analyses of the mitochondrial data recovered similar topologies (Figure 1B), varying in the  
142 *M. thysanodes*, *M. evotis*, and *M. keeni* relationships. Neither method recovered significant support for  
143 these relationships. Bootstrap replicates of the maximum likelihood analysis meet the stopping criterion  
144 after the first 50 of 10,000 replicates (average weighted Robinson-Foulds value = 2.28%). The RAxML  
145 mitochondrial phylogeny was well supported with 29 of 35 nodes present in  $\geq 96\%$  of bootstrap  
146 replicates. The remaining six nodes were present in 47% to 70% of bootstrap replicates. Bayesian  
147 analysis of the mitochondrial data reached convergence, defined as an ASDF of  $<1\%$ , after the first  
148 424,500 of one million generations. The final ASDF, after discarding 25% of samples, was 0.49%. The  
149 trace files from all four independent runs shows proper mixing of samples and the effective sample size  
150 for all parameters was greater than 200. The log likelihood score for the Bayesian mitochondrial tree  
151 was  $-1.205 \times 10^{-5}$  with an ESS of 1,446. In all, posterior probabilities were lower than the bound  
152 established as significant ( $\geq 0.95$ ) for five nodes.

153 Mitochondrial and nuclear analyses recovered different topologies (Figure 1). We stripped  
154 branch lengths from all trees and compared the topologies using an approximately unbiased test to  
155 determine whether differences in the tree represented conflicting signals in the marker sets. When the  
156 nuclear data is constrained to the mitochondrial tree ( $p$ -value =  $1 \times 10^{-66}$ ) or *vice versa* ( $p$ -value =  $2 \times 10^{-5}$ ),  
157 likelihood scores are significantly worse than expected given similar evolutionary histories. These results  
158 reject the hypothesis that the mitochondrial and nuclear UCE phylogenies reflect similar evolutionary  
159 histories.

160 Extended phylogenetic analyses - Many factors can bias phylogenetic analyses resulting in inaccurate  
161 trees (Sanderson and Shaffer 2002). Rather than assuming our initial nuclear UCE tree was an accurate  
162 estimate of the phylogenetic relationships of *Myotis*, we wanted to build a range of plausible topologies  
163 from the nuclear UCE data. To do this we reanalyzed the nuclear UCE data set with minor deviations in  
164 locus sampling, partitioning, inference method, *etc.* In all this effort resulted in 291 unique phylogenetic  
165 analyses. Individual results or topologies are not the focus of these analyses. Rather, the goal was to  
166 recover as many, reasonable, nuclear UCE topologies as possible in an effort to account for phylogenetic

167 uncertainty not present in the initial analysis and to compare the range of nuclear UCE trees to the  
168 mitochondrial genome tree.

169 We investigated the effects of matrix composition (or completeness) on our phylogenetic  
170 inference by generating 10 different alignments having levels of matrix completeness spanning 15-95%  
171 at 10% intervals and including a final matrix of 100% completeness. Loci in these alignments were  
172 partitioned using three separate schemes: all loci were partitioned individually, loci were unpartitioned,  
173 or loci were combined into optimum partitions using PartitionFinder. The result was 10 different  
174 alignments with three partitioning schemes each. These were analyzed using Bayesian and maximum  
175 likelihood methods. Due to computational limits we abandoned the fully partitioned, Bayesian analyses.  
176 The length, number of loci, and optimum number of partitions per alignment is shown in Table 2.  
177 Bootstrap topologies stabilized in 9 of 10 alignments after 50 replicates and all Bayesian runs converged  
178 in less than ten thousand generations. In general, the same alignment produced the same topology  
179 regardless of inference method or partitioning scheme with the only exception being the terminal  
180 relationships *M. levis*/*M. albescens* clade in the optimum vs. unpartitioned Bayesian analysis of the  
181 100% complete data matrix.

182 Trees were generated from data matrices incorporating loci of differing lengths (Hosner, et al.  
183 2016). All 3,648 loci were ordered based on their length and split into nine bins of 365 loci and 1 bin of  
184 363 loci, so that the first bin contained the 365 shortest loci, the second bin contained the 366<sup>th</sup> to the  
185 731<sup>st</sup>, and so on. The number of informative characters per bin ranged from 1,115 to 6,995 and the  
186 number of informative characters was correlated with average locus length (Supplemental Figure 2). On  
187 average, only 2.6% of characters in each bin were parsimony-informative. Each of the ten length-based  
188 alignments recovered slightly different topologies. Terminal relationships were generally stable across  
189 analyses with the majority of differences between topologies found in the early bifurcations of the  
190 ingroup (*Myotis*).

191 From the above analyses combining different matrix composition, inference method,  
192 partitioning, and locus-length variants we observed that, in general, larger alignments produced well  
193 resolved topologies with significant nodal support regardless of the phylogenetic method or partitioning  
194 scheme used. On the other hand, re-analyses of smaller portions of the data were more likely to recover  
195 unique topologies. Given that the overall goal of the extended analyses was to generate as many  
196 reasonable nuclear UCE based topologies for comparison with the mitochondrial tree, we decided to  
197 randomly sample small portions of the nuclear UCE loci to create alignments that are more likely to  
198 result in unique topologies. We randomly subsampled the 3,648 enriched loci to create 100 unique data

199 sets. Loci were concatenated in each replicate data set and analyzed using maximum likelihood in  
200 RAxML. Of the 100 alignments analyzed, 80 unique topologies were generated (mean Robinson-Foulds  
201 distance = 4.3).

202 In addition to concatenated analyses, three summary-based species tree programs were used  
203 on datasets of varying matrix-completeness (ASTRAL-II, ASTRID, SVDquartets). Normalized quartet  
204 scores from ASTRAL-II (Mirarab and Warnow 2015) analyses were quite consistent with scores ranging  
205 from 0.540 to 0.553, and between 7,745,739 (100% complete 212 gene trees) and 63,042,410 (15%  
206 3648 loci) induced quartet gene trees. SVDquartets (Chifman and Kubatko 2014) sampled all 66,045  
207 quartets. On average, the total weight of incompatible quartets was 2.84%. Similar to the concatenated  
208 analysis, we inferred coalescent-based species from the same 100 subsamples of 365 loci described  
209 above. Despite being generated from the same underlying data, summary and concatenation methods  
210 only recovered the same tree in one of 100 attempts.

211 Finally, we used weighted and unweighted statistical binning to combine individual gene trees  
212 into supergenes, estimate the supergene phylogeny, and then infer the species tree from the supergene  
213 trees. The 3,648 loci were combined into 528 binned loci with 480 bins containing seven loci each and  
214 48 bins containing six loci each. Normalized quartet scores were 0.672 for the binned-unweighted and  
215 0.673 for the binned-weighted ASTRAL-II analysis. Given the relative even distribution of loci into bins  
216 the negligible difference in quartet/species tree discordance is expected. Both binning methods  
217 recovered the same topology which was the same tree recovered in the initial nuclear UCE analyses and  
218 was the most common topology observed across all analyses.

219 Topology comparisons – After rejecting topological congruence between the initial nuclear UCE  
220 and mitochondrial phylogenies we used various methods to re-analyze the nuclear UCE data in an effort  
221 to identify alternative nuclear topologies. Topological congruence between the mitochondrial sequence  
222 data and nuclear topologies resulting from the extended analyses were tested to see if any were  
223 statistically congruent with the mitochondrial phylogeny of *Myotis*. Site-log likelihood scores for the  
224 mitochondrial alignments when constrained to all 175 unique nuclear UCE topologies were generated in  
225 RAxML and analyzed in Consel using the Shimodaira-Hasegawa (Shimodaira and Hasegawa 1999) and  
226 approximately unbiased tests (Shimodaira 2002). In each case, the mitochondrial data produced  
227 significantly worse likelihood scores, rejecting congruence between the nuclear UCE and mitochondrial  
228 phylogenies (Supplemental Table 1).

229 When visualizing all topologies in tree space, nuclear trees co-localized and were distinct from  
230 mitochondrial topologies (Figure 2A). Pairwise comparisons of Robinson-Foulds symmetrical differences



231 show that 98.75% of nuclear UCE vs. nuclear UCE (Figure 2B) trees are more similar to each other than  
232 the mitochondrial trees are to even the most similar nuclear UCE tree (Figure 2C). The most frequently  
233 observed topology was recovered in 45 of the 294 nuclear analyses and was identical to the tree  
234 recovered in the initial nuclear UCE analysis (Figure 1a). Of the 45 analyses that recovered the most  
235 frequently observed topology, 38 were Bayesian and RAxML searches that varied by matrix  
236 completeness and partitioning scheme. The fact that these analyses recovered the same topology is  
237 expected given that they are not independent. For example, a RAxML analysis of the 15% complete data  
238 set uses 1.26 Mb of the 1.38 Mb of data from the 25% complete dataset. These two alignments are 91%  
239 identical. Analyses that directly varied the alignments and/or sampled less data (e.g. randomly sampling  
240 loci) were more likely to generate unique topologies than the nested analyses described above. Of the  
241 200 analyses that randomly sampled UCE loci 164 unique topologies were observed. This implies that  
242 when analyses of large data sets produce well-resolved trees with significant nodal support, sampling  
243 smaller portions of the data, may provide a mechanism for creating phylogenetic uncertainty not  
244 represented by typical tree scoring metrics. To account for the phylogenetic uncertainty present in our  
245 dataset, we generated a consensus tree from all nuclear topologies using an 85% threshold to resolve  
246 bipartitions (Figure 3).

## 247 **Discussion**

248 We generated phylogenies from 3,648 UCE loci and mitochondrial genomes of 35 *Myotis* bats.  
249 Initial analyses of the mitochondrial and nuclear UCE phylogenies recovered distinct topologies (Figure  
250 1). Rather than rejecting concordance between the two data types from a single analysis we took steps  
251 to re-analyze the nuclear UCE data in an effort to generate as many viable nuclear topologies as  
252 possible. We recovered 175 unique nuclear topologies using multiple methodologies, sampling  
253 strategies, and parameters. None of these nuclear topologies were similar to the topology produced  
254 from the mitochondrial data suggesting that nuclear UCE loci and the mitochondrial genomes of *Myotis*  
255 have distinct evolutionary histories. The conflict between the mitochondrial and nuclear data may be  
256 driven by error in phylogenetic estimation or may reflect genuine conflict between the two marker types  
257 (Degnan and Rosenberg 2009; Huang, et al. 2010). We relied on multiple tree-inference methods (e.g.  
258 summary vs. concatenation), manipulated phylogenetic parameters (e.g. partitioning strategy), and  
259 sampling criteria (e.g. loci sampled in all taxa) to minimize the impacts of phylogenetic error on the data  
260 set. In most cases, varying parameter or methodologies generated unique topologies, often due to  
261 rearrangements of a few terminal taxa. *M. volans* and *M. brandtii* were often placed as either sister to  
262 the remaining NW *Myotis* or as an early bifurcation between the NA and NT clades. *M. vivesi* was often

263 found as sister to the clade containing *M. lucifugus*, *occultus* and *fortidens* or as sister to the clade  
264 containing the NT *Myotis*.

265         Around 98.3% of all nuclear tree vs. nuclear tree comparisons contain fewer than 30 symmetric  
266 differences (Figure 2b) but there are no mitochondrial vs. nuclear tree comparisons with less than 30  
267 symmetric differences (Figure 2c). Interestingly, the most common nuclear topology most often  
268 recovered by concatenation analyses (Figure 1A). Summary methods failed to recover the most common  
269 nuclear topology except when loci were binned together prior to gene tree estimation. Summary  
270 methods also tended to recover more unique topologies than concatenation methods when analyzing  
271 data from the same gene(s). For example, the random sample analyses recovered 80 unique topologies  
272 using concatenation (RAxML) and 89 unique topologies with summary methods (ASTRAL-II). This likely  
273 has to do with the limited number of informative characters per locus and by extension limited  
274 phylogenetic signal per gene tree (Supplemental Figure 2). In these instances, limited phylogenetic  
275 signal per gene would likely lead to increased opportunity for phylogenetic error in gene tree  
276 estimation. Further supporting this idea, binning of compatible UCE loci may have indirectly increased  
277 phylogenetic signal resulting in the same topology that many of the concatenation analyses recovered.  
278 No other summary/coalescent method recovered this topology.

279         Previous work with UCE loci demonstrated that support for deep divergences varied based on  
280 the number of loci examined (McCormack, et al. 2013). Further, bootstrap replicates and clade  
281 probability values can be inaccurate metrics of nodal support (Douady, et al. 2003; Hedtke, et al. 2006).  
282 Varying the input data and phylogenetic parameters can produce a range of reasonable nuclear  
283 topologies that may be more useful than overreliance on a tree resulting from a one or two analyses.  
284 Here, by considering the different topologies that result from various analyses (e.g. partitioning  
285 strategies, inference methods, etc.), we can account for phylogenetic uncertainty better than  
286 considering a single nuclear or mitochondrial topology alone.

287         The mitochondrial alignment constrained to any of the 175 nuclear topologies generated  
288 significantly worse likelihood scores than expected by chance (Supplemental Table 2) and a comparison  
289 of topologies in tree space shows that the mitochondrial topologies are unique from all nuclear  
290 topologies (Figure 2A). Pairwise tree distances demonstrate that all but the most divergent nuclear  
291 topologies are more similar to each other (Figure 2B) than any nuclear vs. mitochondrial comparison  
292 (Figure 2C). Despite the number of different analyses, the nuclear data never recover a topology that is  
293 similar, much less identical, to the mitochondrial topology.

294 Multiple studies have recovered effectively the same relationships among *Myotis* using  
295 mitochondrial markers to the one presented here (Ruedi and Mayer 2001; Stadelmann, et al. 2007;  
296 Roehrs, et al. 2010; Larsen, et al. 2012; Ruedi, et al. 2013; Haynie, et al. 2016). Thus, we are confident  
297 that the mitochondrial phylogeny we recovered here, and by others, reflects the true mitochondrial  
298 tree. However, the mitochondrial topology may not adequately reflect the species history, particularly  
299 when considering the factors that cause incongruence between nuclear and mitochondrial gene trees.  
300 Possible causes of conflicting gene trees are horizontal transfer, gene duplication, introgressive  
301 hybridization, and incomplete lineage sorting. Some of these phenomena are more likely to have  
302 influenced the *Myotis* radiation than others.

303 Horizontal transfer of genes is thought to be rare in eukaryotes, but, vespertilionids in general  
304 (Thomas, et al. 2011; Platt, et al. 2014), and *Myotis* (Pritham and Feschotte 2007; Ray, et al. 2007; Ray,  
305 et al. 2008) in particular, have experienced horizontal transfer of DNA transposons. These events would  
306 not be reflected in our phylogeny since repetitive sequences were removed prior to phylogenetic  
307 analyses. More generally, gene duplications could create conflicting signal among individual UCE  
308 markers (ex. comparing non-orthologous UCE loci), but the number of gene duplication events would  
309 have to be very high to impact enough of the 3,648 UCE loci to confound the mitochondrial and nuclear  
310 phylogenies. Further ruling out gene duplication events as the dominant cause of conflicting  
311 phylogenetic signal is the fact that such events are likely depressed in *Myotis* as evidenced by their  
312 smaller genome size (~2.2 Gb) and trend towards DNA loss (Kapusta, et al. 2017) combined with low  
313 rates of paralogy in UCEs general (Derti, et al. 2006).

314 Introgressive hybridization and reticulation could significantly influence the phylogenies of  
315 *Myotis* in a way that leads to conflicting signal between the nuclear and mitochondrial genomes (Sota  
316 2002; Good, et al. 2015). Hybridization in bats may be relatively common given their propensity to  
317 swarm at cave entrances for breeding purposes. In European *Myotis*, swarming has allowed for high  
318 degrees of hybridization between *M. brandtii*, *M. mystacinus*, and *M. alcahoie* (Bogdanowicz, et al.  
319 2012). Further, *M. evotis*, *thysanodes*, and *keeni* all experienced historical gene flow during their  
320 divergence (Carstens and Dewey 2010; Morales, et al. 2016). It is also possible to explain the differences  
321 between the mitochondrial and nuclear UCE phylogenies if *Myotis* experienced extensive incomplete  
322 lineage sorting during their radiation. Two factors can influence the rate of lineage sorting, the fixation  
323 rate and the speciation rate (Hudson, et al. 2002). Increasing the time to fixation and/or decreasing the  
324 amount of time between cladogenic events will increase the likelihood of incomplete lineage sorting.  
325 *Myotis* are generally long lived species (Dzeverin 2008) and underwent a rapid radiation between 5-10

326 MYA (Lack, et al. 2010), suggesting that *Myotis* species are likely to experience higher levels of lineage  
327 sorting. The importance of these events -introgressive hybridization and incomplete lineage sorting- in  
328 driving the differences between the mitochondrial and nuclear phylogenies cannot be determined with  
329 the current data.

330 **Evolutionary history of *Myotis*** – Our previous understanding of relationships within *Myotis* is  
331 heavily biased with mitochondrial data because nuclear markers were harder to collect and produced  
332 fewer informative sites (Ruedi and Mayer 2001; Stadelmann, et al. 2007; Lack, et al. 2010; Roehrs, et al.  
333 2010; Larsen, et al. 2012; Ruedi, et al. 2013; Haynie, et al. 2016). Our UCE-based results indicate that  
334 nuclear trees vary substantially from the mitochondrial tree. Given that the nuclear and mitochondrial  
335 trees are different, we find it necessary to re-evaluate *Myotis* in the context of the nuclear data.

336 Paraphyly of *M. nigricans* and *M. albescens* was inferred from previous mitochondrial  
337 phylogenies and confirmed in the UCE tree (Larsen, et al. 2012). Larsen et al (Larsen, et al. 2012)  
338 identified a minimum of four and potentially twelve lineages in *M. albescens* and *M. nigricans*. Our  
339 sampling included four *M. albescens* and three *M. nigricans*, compared to Larsen's 17 and 29 samples.  
340 Despite different mitochondrial and nuclear topologies overall, our mitochondrial and nuclear  
341 phylogeny recovered the same paraphyletic clade of three *M. albescens* samples and *M. levis*. Close  
342 relationships between these taxa was found in previous work and expected. More importantly we did  
343 not find that *M. albescens* was paraphyletic across much of NT *Myotis*. We also found that *M. nigricans*  
344 is monophyletic in the nuclear tree, but paraphyletic in the mitochondrial tree. These results from *M.*  
345 *nigricans* and *M. albescens* are interesting but further inference is limited due to low sample sizes for  
346 these taxa.

347 The original subgeneric taxonomy of *Myotis* was based on three morphotypes that were later  
348 shown to be the result of convergent evolution (Ruedi and Mayer 2001). If lineage-sorting affected the  
349 mitochondrial phylogeny, it is possible that the morphotypes truly are monophyletic. However,  
350 superimposing the previous subgeneric/morphological classification onto the species tree shows  
351 interspersed distribution of morphotypes throughout even the most conservative nuclear tree (Figure  
352 3). Many strongly supported terminal relationships link species with different morphotypes. Based on  
353 these results, it appears that the three major morphotypes in *Myotis* are indeed a result of convergent  
354 evolution, as suggested by previous work (Ruedi and Mayer 2001; Stadelmann, et al. 2007).

355 Among the more dramatic differences between the nuclear and mitochondrial topologies is the  
356 placement of *M. volans* and *M. brandtii* as sister to all New World taxa by the nuclear data. Our  
357 mitochondrial analyses place *M. volans* within a Nearctic clade and *M. brandtii* directly in-between the

358 Nearctic and Neotropical bifurcations as has been previously reported (Stadelmann, et al. 2007). Clade  
359 probability values and bootstrap frequencies support these placements in trees from both data types.  
360 Our placement of *M. brandtii* as sister to all other New World *Myotis* more closely affiliates it with Old  
361 World taxa. This make sense given that the *M. brandtii* distribution is also Old World. On the other hand,  
362 a placement of *M. volans* sister to all New World taxa (and *M. brandtii*) in the nuclear tree is a significant  
363 departure from previous work and, at first glance, does not make as much sense in a biogeographic  
364 framework. *M. volans* is distributed across western and northwestern North America as far as far north  
365 as Alaska. *M. brandtii* is distributed across much of Northern Europe. The key may lie in understanding a  
366 third species, *M. gracilis*.

367 *M. gracilis*, along with *M. brandtii*, are the only two *Myotis* geographically distributed in the Old  
368 World, but phylogenetically affiliated with the New World (Stadelmann, et al. 2007). If the sister  
369 relationship between *M. brandtii* and *M. gracilis* (not sampled here) holds when nuclear data are  
370 examined, then we can envision a scenario where *M. gracilis*, *M. brandtii*, and *M. volans* represent  
371 speciation events that occurred during the transition of *Myotis* from the Old World to the New World. It  
372 is important to remember that this interpretation relies on a fairly dramatic departure from the  
373 currently accepted mitochondrial relationships of *M. volans* (represented here by a single sample) to  
374 other *Myotis* species, and this hypothesis should be viewed as highly speculative. Increasing the number  
375 of *Myotis* lineages sampled will shed additional light on this hypothesis.

376 Other taxa with conflicting positions between datasets include *M. lucifugus* + *M. occultus*, *M.*  
377 *fortidens*, and *M. vivesi*. In general, these relationships are characterized by very short branches and are  
378 the most likely to be affected by incomplete lineage sorting or limited phylogenetic information. This  
379 could explain the strong support with the mitochondrial tree compared to the nuclear species tree,  
380 while allowing for a number of nuclear loci to disagree with the species tree, as well.

381 There are a number of monophyletic groups identified with nuclear data (Fig. 1A) that exhibit  
382 distinct biological characteristics. For example all of the long eared bats (*septentrionalis*, *auriculus*,  
383 *evotis*, *thysanodes* and *keenii*) represent a monophyletic group of higher elevation, forest-dwelling  
384 species that glean insects off of surfaces (Fitch and Shump 1979; O'Farrell and Studier 1980; Warner  
385 1982; Manning and Jones 1989; Caceres and Barclay 2000). The group represented by *fortidens*,  
386 *lucifugus* and *occultus* represent a relatively long-haired form of *Myotis*. While having a distinct dental  
387 formula, *fortidens* was historically described as a subspecies of *M. lucifugus* (Miller Jr and Allen 1928)  
388 and *occultus* has alternately represented its own species or been considered a subspecies of *lucifugus*  
389 (Hollister 1909; Valdez, et al. 1999; Piaggio, et al. 2002). The clade consisting of *keaysi*, *oxyotus*, *ruber*,

390 *simus*, *riparius*, *albescens* and *diminutus* represents a NT group of primarily woolly-haired bats (LaVal  
391 1973). If the mitochondrial genome has been subjected to phenomena that obscure the true species  
392 tree then these species groups, along with their synapomorphic morphological features, can be  
393 reevaluated.

394 **Conclusion** - Relationships within *Myotis*, which until now have relied heavily on mitochondrial  
395 data, have served as the basis for species identification (Puechmaille, et al. 2012), evolutionary  
396 hypotheses (Simões, et al. 2007), and even conservation recommendations (Boyles and Storm 2007).  
397 Previous studies using nuclear data have largely been uninformative or utilized too few samples to draw  
398 definitive conclusions. Trees estimated from ~3,650 nuclear loci and 295 different phylogenetic analyses  
399 recovered 175 topologies, none of which are congruent with the mitochondrial phylogeny of *Myotis*.  
400 Conflict between the mitochondrial and nuclear trees as well as among individual nuclear loci suggest  
401 that the *Myotis* radiation may have been accompanied by high levels of incomplete lineage sorting and  
402 possible hybridization. Rather than placing emphasis on the mitochondrial tree, it may be more  
403 appropriate to consider it for what it really is: a single gene on par with a single UCE locus, albeit one  
404 with many more phylogenetically informative characters. If true, then the mitochondrial genome is as  
405 likely to reflect the true species tree as any UCE locus chosen at random. Large amounts of lineage  
406 sorting make phylogenetic inference difficult and potentially impossible. Other phenomena such as  
407 reticulation, hybridization, and introgression have likely influenced the genomes of *Myotis* and should  
408 be accounted for in subsequent work. It is possible that the *Myotis* radiation is more accurately reflected  
409 as a hard polytomy or a phylogenetic network rather than a strictly bifurcating phylogeny.

410

#### 411 **Materials and Methods:**

412 Taxon Selection - Taxa were selected to span the major phylogenetic break points with emphasis  
413 on the Nearctic and Neotropical bifurcation as recovered in previous mitochondrial phylogenies  
414 (Stadelmann, et al. 2007; Ruedi, et al. 2013) (Table 1). In addition, multiple individuals morphologically  
415 identified as *M. nigricans* and *M. albescens* were included to test paraphyly as demonstrated by Larsen  
416 et al. (2012). Three Old World species of *Myotis* and the outgroup, *E. fuscus*, were included to root  
417 phylogenetic analyses. All field identifications were confirmed from voucher specimens. Information for  
418 all specimens examined is available in Table 1.

419 UCE preparation, sequencing, and processing - Genomic DNA was extracted from 33 samples  
420 using either a Qiagen DNEasy extraction kit or a phenol-chloroform/ethanol precipitation. DNA was  
421 fragmented using the Bioruptor UCD-300 sonication device (Diagenode, Denville, NJ, USA). Libraries

422 were prepared using the Kapa Library Preparation Kit KR0453-v2.13 (Kapa Biosystems, Wilmington, MA,  
423 USA) following the manufacturer's instructions with five minor modifications. First, we used half volume  
424 reactions. Second, subsequent to end repair, we added Sera-Mag Speedbeads (Thermo-Scientific,  
425 Waltham, MA, USA; prepared according to (Glenn, et al. 2016)) at a ratio of 2.86:1 for end repair  
426 cleanup. Third, we ligated universal iTru y-yoke adapters (Glenn, et al. 2016) onto the genomic DNA.  
427 Fourth, following adapter ligation, we performed one post-ligation cleanup followed by Dual-SPRI size  
428 selection using 55  $\mu$ L of speedbead buffer (22.5mM PEG, 1M NaCl) and 25  $\mu$ L of Speedbeads. Finally, we  
429 performed a PCR at 95 °C for 45 sec, then 14 cycles of 98 °C for 30 sec, 60 °C for 30 sec, 72 °C for 30sec,  
430 then 72 °C for a 5 minute final extension and a 12 °C hold using iTru5 and iTru7 primers to produce  
431 Illumina TruSeqHT compatible libraries (Glenn, et al. 2016).

432 Libraries were quantified on a Qubit 2.0 (Life Technologies) and 83 ng from each library was  
433 added to create 5 pools of 6 or 7 libraries each. We then split the pools in two. One subsample was  
434 enriched for UCE loci, the other was not. UCE loci in the enriched library pools were captured using  
435 Tetrapods 5K version 1 baits from MYcroarray (Ann Arbor, MI, USA) following their MYbaits protocol v.  
436 2.3.1 with overnight incubations (Faircloth, et al. 2012). Enriched libraries were quantified with a Qubit  
437 and pooled with other unrelated samples prior to sequencing on an Illumina HiSeq 3000 to produce  
438 paired-end reads of  $\leq$  151 bases. The unenriched samples were sequenced on a separate run using a  
439 single lane of Illumina HiSeq 2500. All samples were demultiplexed with Illumina software fastq2bcl.  
440 Reads were quality filtered by removing any potential adapter sequence and trimming read ends once  
441 the average Phred quality over a four base window score dropped below 20 using the Fastx toolkit  
442 (Gordon and Hannon 2010).

443 Quality filtered raw sequence reads were assembled into contigs using the Trinity assembler  
444 (Grabherr, et al. 2011) and a minimum kmer coverage of 2, and we used Phyluce to identify those  
445 assembled contigs that were UCE loci. We also harvested UCE loci from *Eptesicus fuscus*  
446 (GCA\_000308155.1), *Myotis brandtii* (GCA\_000412655.1), *M. davidii* (GCA\_000327345.1), and *M.*  
447 *lucifugus* (GCF\_000147115.1) genome assemblies using the Phyluce package (Faircloth 2016). Once  
448 extracted from Trinity and genome assemblies, we aligned all UCE loci MAFFT (Katoh, et al. 2002),  
449 trimmed the aligned data with gBlocks (Castresana 2000). Repetitive sequences (i. e. transposable  
450 elements) in each alignment were identified with RepeatMasker and trimmed where found.

451 Mitochondrial genome assembly and annotation – Raw reads from the unenriched libraries  
452 were used to generate mitochondrial genomes via MitoBim (Hahn, et al. 2013) in most cases. This  
453 program used MIRA (B, et al. 1999) to map reads to a *M. brandtii* reference genome (Genbank accession

454 number KT210199.1). Alternative methods of mitochondrial genome assembly were used when  
455 MitoBim assembly failed. These taxa include *M. albescens* (TK61766), *M. albescens* (TK 101723), *M.*  
456 *albescens* (RDS 7889), *M. fortidens*, *M. keeni*, *M. melanorhinus*, *M. nigricans* (QCAZ 9601), *M.*  
457 *septentrionalis*, *M. simus*, *M. velifer*, and *M. volans*. For these samples, we first identified reads that  
458 were mitochondrial in origin using BLAST searches against the *M. brandtii* mitochondrial genome  
459 (KT210199.1). Those reads were assembled using Trinity v2.2.0 with the `-single` option. For taxa where  
460 we either could not assemble useable mitochondrial genomes, we retrieved proxy data from GenBank  
461 as follows: *M. brandtii* (KT210199.1), *E. fuscus* (KF111725.1), *M. lucifugus* (KP273591.1), and *M. davidii*  
462 (KM233172.1).

463         Once assembled, each mitogenome was annotated via MITOS (Bernt, et al. 2013). Annotated  
464 genes were manually validated via BLAST to confirm sequence identity and length. Protein coding genes  
465 were checked for stop codons using EMBOSS's transeq program (Rice, et al. 2000). When a stop codon  
466 was found, we used the raw reads to verify the sequence. We used BWA v0.7.12 (Li and Durbin 2009) to  
467 align the reads to the Mitobim assembled mitogenome to verify base calls from Mitobim. The protein  
468 coding rRNA and tRNA genes from each assembly were aligned using MUSCLE and concatenated into a  
469 single alignment for phylogenetic analyses, as described below.

470         Initial phylogenetic analyses - Initial phylogenies derived from UCE loci and mitochondrial coding  
471 regions were generated using maximum likelihood and Bayesian methodologies. For the first round of  
472 phylogenetic analyses all UCE loci present in 20 or more taxa were concatenated into a single alignment.  
473 PartitionFinder v1.1.1 (Lanfear, et al. 2012) was used to identify and combine loci into an optimal  
474 partitioning scheme using the hcluster heuristic algorithm. We assumed a GTR+ $\Gamma$  model for all loci  
475 (Darriba and Posada 2015). Initial trees were generated using RAxML v7.4.1 (Stamatakis 2006) with  
476 linked branch lengths RaxML (v8.1.3) was used to estimate and score the maximum likelihood phylogeny  
477 with the rapid bootstrapping option and 1,000 bootstrap replicates. We define strongly supported  
478 bipartitions as those present in 95-100% of bootstrap replicates and moderately supported bipartitions  
479 are present in 85-95% of bipartitions (Wiens, et al. 2008). A Bayesian phylogeny was generated with the  
480 MPI version of ExaBayes (v1.4.1) using two independent runs of 4 chains each. ExaBayes runs were  
481 terminated after 1 million generations only if the average standard deviation of split frequencies was  
482 less than 0.01. The first 25% of samples were discarded after which every 100<sup>th</sup> generation was sampled.  
483 The `"-M 3"` option was used to reduce the memory footprint of all ExaBayes runs. Proper sampling, post  
484 burn-in was inspected via Tracer v1.6. (Rambaut, et al. 2014). Effective sample sizes greater than 200



485 were considered acceptable. Posterior probability values greater than 95% were considered to be  
486 significant.

487 The mitochondrial phylogeny was generated using methods similar to those described above  
488 with the following exceptions. All 37 coding regions, including protein coding genes, tRNA and rRNAs,  
489 were concatenated into a single alignment. Genes were partitioned individually except in the instances  
490 where two genes overlapped. These regions were partitioned separately from the individual genes  
491 resulting in three partitions for the two genes: a partition for gene A, a partition for gene B, and a  
492 partition for the overlapping nucleotides of gene A and B. The fast bootstrapping search in RAxML was  
493 run for 10K replicates and Bayesian analyses were performed across four independent runs with four  
494 chains of ten million generations.

495 The mitochondrial and nuclear phylogenies were compared to each other to identify  
496 discordance between marker types. Site-log likelihood scores were calculated for the mitochondrial  
497 alignments when constrained to the nuclear tree while the nuclear alignment was scored against the  
498 mitochondrial tree using RAxML. Model parameters were then recalculated for each constrained  
499 alignment (-f G). Site-log likelihood scores were analyzed using CONSEL (Shimodaira and Hasegawa  
500 2001) and compared using the approximately unbiased test (Shimodaira 2002). P-values less than 0.05  
501 were used to indicate that the trees produced by mitochondrial or nuclear data differed.

502 *Extended phylogenetic analyses* - Many factors can influence phylogenetic inference. To reduce  
503 the likelihood of any single factor influencing the results, we re-examined the nuclear UCE dataset using  
504 the strategies described below. A flow chart of analyses is available in Supplemental Figure 1.

505 Aligned UCE loci were binned based on the number of taxa represented in the alignment  
506 (`phyluce_align_get_only_loci_with_min_taxa`; Faircloth 2016), or degree of completeness. Groups  
507 included loci present in 100% (number of specimens (n) = 37), 95% (n = 35), 85% (n = 31), 75% (n = 27),  
508 65% (n = 24), 55% (n = 20), 45% (n = 16), 35% (n = 12), 25% (n = 9), and 15% (n = 5) of specimens  
509 examined. These 10 groups were non-exclusive, so a locus that was assembled in all specimens (100%  
510 complete) would also be included with loci present in only 55% of specimens. On the other hand, a locus  
511 found in only 55% of specimens would not be included in the 100% complete data set. Each set of UCE  
512 alignments was concatenated using `phyluce_align_format_nexus_files_for_raxml` and a nexus character  
513 block was created using the `phyluce_align_format_nexus_files_for_raxml -charsets` option. These  
514 datasets then served as the basis for downstream phylogenetic analyses. For example, when a  
515 partitioning methodology (discussed below) was tested, it was performed for each of the 100%, 95%,

516 85%, etc. alignments. In addition to partitioning schemes, the effect of missing data was examined using  
517 Bayesian and maximum likelihood methods.

518 Concatenated alignments were analyzed using three different partitioning schemes.  
519 Unpartitioned alignments were simply concatenated UCE loci treated as a single genetic unit (No  
520 Partitions). Fully partitioned alignments were concatenated alignments of UCE loci that were partitioned  
521 by locus (All Partitions). Finally, PartitionFinder v1.1.1 (Lanfear, et al. 2012) was used to combine  
522 individual loci into an optimal partitioning scheme (Optimal Partitions). Rather than searching for best-  
523 fit substitution models for each UCE locus or partition, the GTR+ $\Gamma$  model of sequence evolution was  
524 assigned to all loci (Darriba and Posada 2015). Initial trees for PartitionFinder were generated using  
525 RAxML v7.4.1 (Stamatakis 2006) with linked branch lengths. Partitioning schemes were heuristically  
526 searched using the hcluster algorithm.

527 Maximum likelihood trees were inferred for the concatenated alignments using RAxML v8.1.3  
528 (Stamatakis 2014). The three partitioning schemes (described above) were applied to each analysis. The  
529 best scoring (lowest -lnL) tree from each dataset was identified from 100 random starting trees and  
530 bootstrapped 100 times using the GTR+ $\Gamma$  in both cases. The autoMRE function in RAxML v8.1.3 was used  
531 to determine the need for additional bootstrap replicates beyond the initial 100 (Pattengale, et al.  
532 2009). A stopping criterion was set *a priori* if the weighted Robinson-Foulds distance was less than 5% in  
533 95% of random permutations of computed bootstrap replicates (Pattengale, et al. 2009). If necessary, an  
534 additional 100 bootstrap replicates were computed until the convergence stopping criteria were met.  
535 Finally, bipartition frequencies of bootstrap replicates were drawn onto the best scoring tree from the  
536 initial RAxML searches for each of the respective data sets.

537 Bayesian analyses were conducted using ExaBayes v1.4.1 (Aberer, et al. 2014). For all Bayesian  
538 analyses four independent runs of four chains each were run in parallel for a minimum of one hundred  
539 thousand generations sampling every thousandth generation and applying a GTR+ $\Gamma$  substitution model  
540 for each partition. Two of the partitioning schemes (described above) were used for each analysis: No  
541 Partitions and Optimal Partitions. After one hundred thousand generations, analyses continued until the  
542 standard deviation of the split frequency between chains was less than 0.01. An extended majority rule  
543 consensus tree was created from all trees after the first 25% of trees were discarded using  
544 TreeAnnotator v1.7.0 (Rambaut and Drummond 2013) and parameter estimates across all runs were  
545 calculated with Tracer v1.6 (Rambaut, et al. 2014).

546 *Sampling loci by number of informative characters* – Previous coalescent analyses of UCE data  
547 have shown that sub-sampling the most informative loci can result in different topologies (Meiklejohn,

548 et al. 2016). Under these assumptions, UCE loci were sorted into ten groups based on their length and  
549 the predicted correlation between length and number of informative characters was confirmed  
550 (Supplemental Figure 2). UCE loci in the same size cohort were combined into a single alignment. Rather  
551 than using coalescent based analyses we used concatenation of UCE loci to identify different topologies  
552 based on length. UCE loci were individually partitioned and the maximum likelihood tree was estimated  
553 with the rapid bootstrapping option in RaxML (bootstrap replicates = 100) using the GTR+ $\Gamma$  substitution  
554 model.

555 *Random sampling of loci* – In large phylogenetic analyses, systematic error can result in highly  
556 supported, but incorrect topologies as a result of compounding non-phylogenetic signal (Rodríguez-  
557 Ezpeleta, et al. 2007). By randomly reducing the dataset and replicating the ML analyses, we can reduce  
558 the potential effects of compounding error. Roughly 10% of the dataset, 365 loci, were randomly  
559 sampled and concatenated to create 100 new alignments. ML methods were similar to those used when  
560 sampling loci by the number of informative characters.

561 *Summary methods* – Gene trees for individual UCE loci recovered in five or more taxa were  
562 inferred using the GTR+ $\Gamma$  substitution model and fast bootstrapping (-f a) option in RAXML (replicates =  
563 1,000). In general, gene trees were classified based on the degree of completeness (i.e. number of taxa  
564 represented) similar to the way we treated individuals as described above.

565 Species trees were estimated and bootstrapped using three different programs. ASTRAL-II v4.10  
566 (Mirarab and Warnow 2015) was used to build a summary tree. Support values for bipartitions in the  
567 tree were generated from 100 bootstrap replicates using site as well as site and locus resampling (Seo  
568 2008). Species trees were estimated from ASTRID v1.4 (Vachaspati and Warnow 2015) using bionj and  
569 bootstrapped for 100 replicates. SVDquartets (Chifman and Kubatko 2014), as implemented in PAUP  
570 v4.0a150 (Swofford 2003), was used to estimate a species trees from a random subset of 200,000  
571 quartets and 1,000 bootstrap replicates.

572 Errors in gene tree estimation may reduce the accuracy of summary methods (Liu, et al. 2009;  
573 Leaché and Rannala 2011; DeGiorgio and Degnan 2014; Mirarab, et al. 2016). We used weighted (Bayzid,  
574 et al. 2015) and unweighted (Mirarab, et al. 2014) statistical binning to combine gene trees into  
575 compatible supergenes using the pipeline available in Bayzid et al. (Bayzid, et al. 2015). The gene trees  
576 used for the summary tree methods described above were used rather than re-estimating trees.  
577 Bifurcations supported by more than 50% of the bootstrap replicates were retained for each gene tree.  
578 Alignments from compatible trees were concatenated into a single supergene alignment. Trees for  
579 supergenes were estimated using RAXML. The best trees for each supergene, as defined by log

580 likelihood score, were retained from 500 searches. Bipartition support was estimated from 500  
581 bootstrap replicates. For all analyses, the GTR+ $\Gamma$  model of substitution was used and each gene in the  
582 supergene alignment was partitioned separately. The resulting supertrees were then used for species  
583 tree estimation using ASTRAL-II. For the unweighted analysis, all supertrees were included in the pool of  
584 trees. For the weighted analysis, supertrees were weighted according to the number of genes combined  
585 in the supergene alignment. For example, if a supergene was a composite of six genes, the supertree  
586 was present 6 times compared to a composite of five genes which would be represented only five times.  
587 Support for the weighted and unweighted species trees was estimated by site and site and locus re-  
588 sampling (Seo 2008) for 100 bootstrap replicates in ASTRAL-II.

589 *Meta-analyses* - Trees recovered from all analyses were compared to each other in tree space.  
590 Unweighted Robinson-Foulds distances were calculated among all trees. This distance matrix was  
591 transformed into two dimensions using the stochastic CCA algorithm for nonlinear dimension reduction  
592 in TreeScaper v1.09 (Huang, et al. 2016). Coordinates were then visualized in R using hexagonal binning  
593 in the hexbin library v1.27.1 (Lewin-Koh 2011).

594 We compared the mitochondrial data to all nuclear trees. Branch lengths have different  
595 meanings based on the type of analysis. For example, ASTRAL-II branch lengths are representative of  
596 coalescent units. ASTRID doesn't even calculate branch lengths. For accurate tree comparisons, branch  
597 lengths were stripped from all trees using regular expressions and Sed. Site log-likelihood scores were  
598 calculated for each nuclear tree, without branch lengths, and using the mitochondrial alignment. Model  
599 parameters were re-estimated for each tree. Site-log likelihood scores were compared with the  
600 approximately unbiased (Shimodaira 2002) and Shimodaira-Hasegawa (Shimodaira and Hasegawa 1999)  
601 test in CONSEL and values less than 0.05 were indicative of differences. Finally, we used RAxML to  
602 generate a 85% and majority rule consensus trees from all nuclear trees.

603

#### 604 **Acknowledgments:**

605 We would like to thank the following museums, collection managers, and collaborators for the  
606 tissue loans necessary to complete this work: Joseph Cook (Museum of Southwestern Biology), Museum  
607 of Vertebrate Zoology, Manuel Ruedi (Natural History Museum of Geneva), Santiago Burneo (Pontificia  
608 Universidad Catolica del Ecuador Museo de Zoologia), Heath Garner, Robert Bradley and Caleb Phillips  
609 (Texas Tech University Natural Science Research Laboratory), Link Olson (University of Alaska Museum  
610 of the North), Cody Thompson and Priscilla Tucker (University of Michigan Museum of Zoology). In  
611 addition, we would like to thank the Texas Tech HPCC ([www.hpcc.ttu.edu](http://www.hpcc.ttu.edu)) for providing the

612 computational resources necessary to complete this project. This work was supported by the National  
613 Science Foundation, DEB-1355176. Additional support was provided by College of Arts and Sciences at  
614 Texas Tech University. All sequence data is available at NCBI's Short Read Archive (SRP095250). UCE  
615 contig assemblies are available at (PENDING ACCESSION NUMBER). A supplemental file contains all  
616 estimated species trees in nexus format (supMaterial-AllTrees-nexus.txt). Individual UCE alignments in  
617 fasta format and an archived file containing all individual UCE gene trees in Newick format is available  
618 through Dryad (PENDING ACCESSION NUMBER).  
619

620 **Figure and Table Captions**

621 **Figure 1.** Comparison of nuclear and mitochondrial phylogenetic trees in *Myotis*. Bayesian trees  
622 generated from (A) 2,890 nuclear UCE loci and (B) 37 mitochondrial protein, tRNA, and rRNA genes (B)  
623 Posterior probability values greater than 0.95 are shown as a “\*”. Values below branches are  
624 percentages of maximum likelihood bootstrap replicates supporting that clade. Conflicting tips between  
625 data types (nuclear vs. mitochondrial) are indicated with lines between the topologies. The  
626 mitochondrial Bayesian and maximum likelihood trees resolved different relationships among *M.*  
627 *thysanodes*, *evotis*, and *keeni* as indicated by the dotted lines. Species with more than one sample are  
628 designated with a superscript that is referenced in Table 1. Specimens derived from whole genome  
629 alignments are designated with a superscript “G”.

630 **Figure 2.** Differences between mitochondrial and nuclear topologies. (A) All trees recovered from  
631 mitochondrial genes and the extended analysis of the nuclear data were visualized in tree space using  
632 multidimensional scaling. Nuclear trees (green) were distinct from mitochondrial trees forming a large  
633 cluster. Most nuclear trees were found within a limited region of tree space. Mitochondrial trees (blue)  
634 were distinct from any of the 294 nuclear trees recovered. Tree vs tree comparisons show that most (B)  
635 nuclear trees are more similar to each other than they are to (C) mitochondrial trees. Symmetric  
636 differences are equal to twice the Robinson-Foulds distance between two trees.

637 **Figure 3.** Consensus tree. A consensus tree of New World *Myotis* was generated from 294 nuclear  
638 topologies with a threshold cutoff of 85%. Values shown above the branches represent the percentage  
639 of nuclear analyses that support a given bipartion. Previous subgeneric classifications based on  
640 morphology are listed at each tip (*Myotis* “M”, *Selysius* “S”, *Leuconoe* “L”. Biogeographic regions are  
641 color coded. Species with more than one sample are designated with a superscript that is referenced in  
642 Table 1. Specimens derived from whole genome alignments are designated with a superscript “G”. This  
643 consensus tree represents a very conservative estimate of the *Myotis* radiation.

644 **Table 1.** Specimens examined.

645 Collection abbreviations: Museum of Southwestern Biology (MSB), Museum of Vertebrate Zoology  
646 (MVZ), Natural History Museum of Geneva (MHNG), Pontificia Universidad Catolica del Ecuador Museo  
647 de Zoologia (QCAZ), Texas Tech University Natural Science Research Laboratory (TK), University of Alaska  
648 Museum of the North (UAM), University of Michigan Museum of Zoology (UMMZ)

649 **Table 2.** General alignment information. For a subset of analyses a series of alignments were generated  
650 based on the number of taxa per locus. Thirty-seven taxa were examined so an alignment with all 37  
651 taxa was considered 100% complete. Parsimony-informative characters make up a small portion of the  
652 total alignment. The optimum partitioning scheme was calculated with PartitionFinder.

653 **Sup Fig 1.** Analytical flow chart. In the initial analysis (A) mitochondrial and nuclear data were analyzed  
654 using Bayesian and maximum likelihood methods. Trees were compared using the approximately  
655 unbiased and the Shimodaira-Hasegawa tests and determined to be conflicting. Extended analysis (B) of  
656 the data used multiple methods and sampling strategies to generate 292 different phylogenetic  
657 inferences. (C) All nuclear and mitochondrial trees were compared in tree space and with topological  
658 tests. An 85% meta-consensus tree from all analyses was used to represent a conservative estimate of  
659 the *Myotis* radiation. Trees from the extended analysis were compared to the mitochondrial trees using  
660 the approximately unbiased and the Shimodaira-Hasegawa tests and determined to be conflicting.

661 **Sup Fig 2.** UCE loci sorted by length. The length of a UCE locus is correlated with the number of  
662 phylogenetically informative characters. UCE loci were sorted by length and ten bins of alignments were  
663 created so that the shortest loci were combined into one alignment, the next shortest set of loci were  
664 combined ... etc. Parsimony informative characters made up a minor part of each alignment.

665 **Sup Table 1.** Tree topology tests. Trees were compared to each other using the approximately unbiased  
666 and the Shimodaira-Hasegawa tests. Likelihood scores were calculated for the mitochondrial alignment  
667 when constrained to all topologies (mitochondrial and nuclear) recovered herein. Alignment and tree  
668 topology incompatibility were identified as p-values < 0.01.

669 **Sup File** -AllTrees-nexus.txt – Trees generated from all analyses in nexus format.

670 **Literature Cited**

- 671 Aberer AJ, Kobert K, Stamatakis A. 2014. ExaBayes: Massively parallel Bayesian tree inference for the  
672 whole-genome era. *Molecular Biology and Evolution* 31:2553-2556.
- 673 Genome sequence assembly using trace signals and additional sequence information [Internet]. 1999 1  
674 August 2015]. Available from: <http://www.bioinfo.de/isb/gcb99/talks/chevreux/main.html>
- 675 Bayzid MS, Mirarab S, Boussau B, Warnow T. 2015. Weighted statistical binning: Enabling statistically  
676 consistent genome-scale phylogenetic analyses. *PLoS ONE* 10:e0129183.
- 677 Bernt M, Donath A, Jühling F, Externbrink F, Florentz C, Fritzschn G, Pütz J, Middendorf M, Stadler PF.  
678 2013. MITOS: Improved de novo metazoan mitochondrial genome annotation. *Molecular*  
679 *Phylogenetics and Evolution* 69:313-319.
- 680 Bogdanowicz W, Piksa K, Tereba A. 2012. Hybridization hotspots at bat swarming sites. *PLoS ONE*  
681 7:e53334.
- 682 Boyles JG, Storm JJ. 2007. The perils of picky eating: Dietary breadth is related to extinction risk in  
683 insectivorous bats. *PLoS ONE* 2:e672.
- 684 Caceres MC, Barclay RMR. 2000. *Myotis septentrionalis*. *Mammalian Species*:1-4.
- 685 Carstens BC, Dewey TA. 2010. Species delimitation using a combined coalescent and information-  
686 theoretic approach: An example from North American *Myotis* bats. *Systematic Biology* 59:400-414.
- 687 Castresana J. 2000. Selection of conserved blocks from multiple alignments for their use in phylogenetic  
688 analysis. *Molecular Biology and Evolution* 17:540-552.
- 689 Chifman J, Kubatko L. 2014. Quartet inference from SNP data under the coalescent model.  
690 *Bioinformatics* 30:3317-3324.
- 691 Crawford NG, Faircloth BC, McCormack JE, Brumfield RT, Winker K, Glenn TC. 2012. More than 1000  
692 ultraconserved elements provide evidence that turtles are the sister group of archosaurs. *Biology*  
693 *Letters* 8:783-786.
- 694 Darriba D, Posada D. 2015. The impact of partitioning on phylogenomic accuracy.
- 695 DeGiorgio M, Degnan JH. 2014. Robustness to divergence time underestimation when inferring species  
696 trees from estimated gene trees. *Systematic Biology* 63:66-82.
- 697 Degnan JH, Rosenberg NA. 2009. Gene tree discordance, phylogenetic inference and the multispecies  
698 coalescent. *Trends in Ecology & Evolution* 24:332-340.
- 699 Derti A, Roth FP, Church GM, Wu Ct. 2006. Mammalian ultraconserved elements are strongly depleted  
700 among segmental duplications and copy number variants. *Nat Genet* 38:1216-1220.
- 701 Douady CJ, Delsuc F, Boucher Y, Doolittle WF, Douzery EJP. 2003. Comparison of Bayesian and maximum  
702 likelihood bootstrap measures of phylogenetic reliability. *Molecular Biology and Evolution* 20:248-254.
- 703 Dzeverin I. 2008. The stasis and possible patterns of selection in evolution of a group of related species  
704 from the bat genus *Myotis* (Chiroptera, Vespertilionidae). *Journal of Mammalian Evolution* 15:123-  
705 142.
- 706 Edwards S, Bensch S. 2009. Looking forwards or looking backwards in avian phylogeography? A  
707 comment on Zink and Carrowclough 2008. *Molecular Ecology* 18:2930-2933.
- 708 Faircloth BC. 2016. PHYLUCE is a software package for the analysis of conserved genomic loci.  
709 *Bioinformatics* 32:786-788.
- 710 Faircloth BC, Branstetter MG, White ND, Brady SG. 2015. Target enrichment of ultraconserved elements  
711 from arthropods provides a genomic perspective on relationships among Hymenoptera. *Molecular*  
712 *Ecology Resources* 15:489-501.
- 713 Faircloth BC, McCormack JE, Crawford NG, Harvey MG, Brumfield RT, Glenn TC. 2012. Ultraconserved  
714 elements anchor thousands of genetic markers spanning multiple evolutionary timescales. *Systematic*  
715 *Biology*:sys004.
- 716 Findley JS. 1972. Phenetic relationships among bats of the genus *Myotis*. *Systematic Biology* 21:31-52.

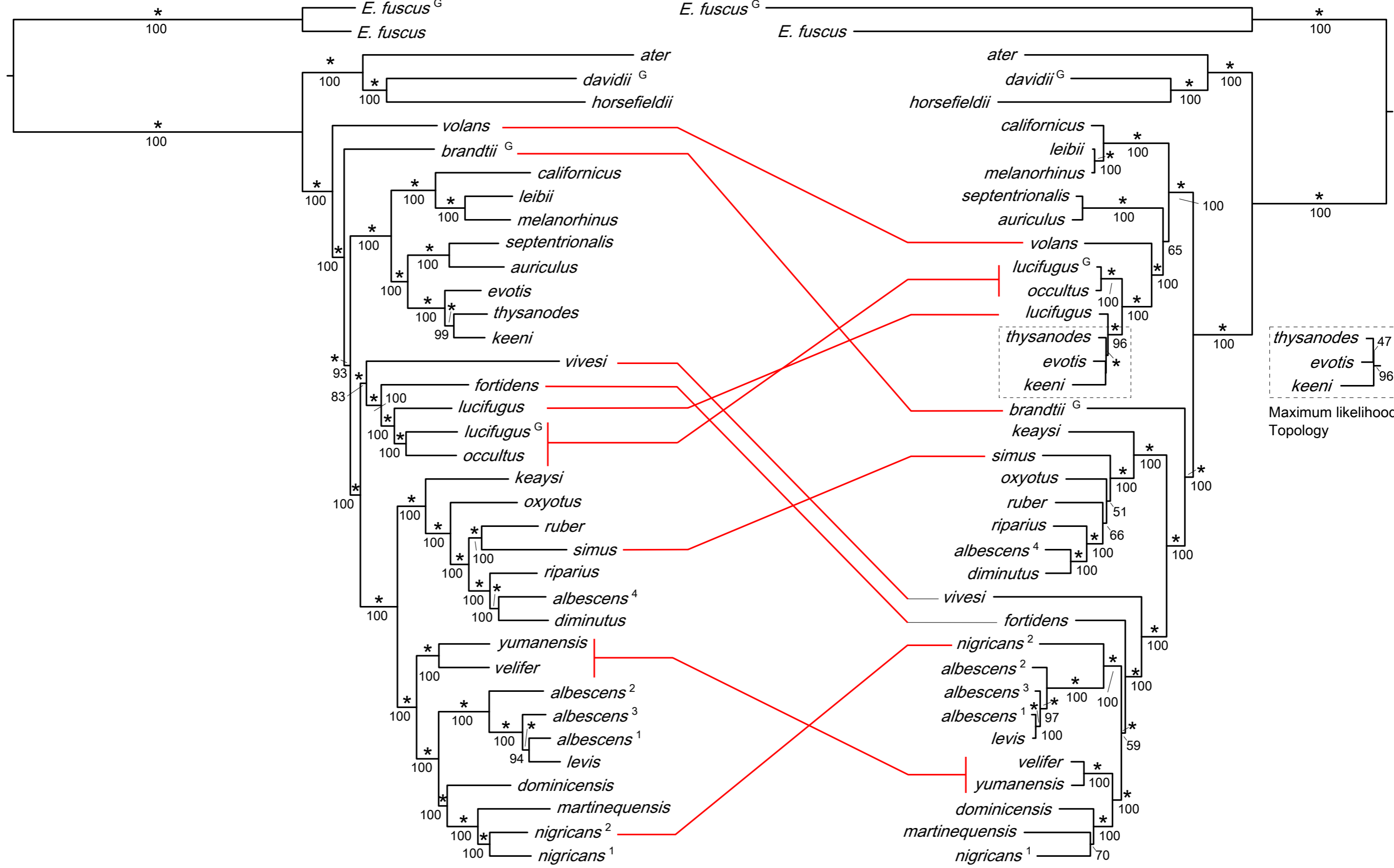
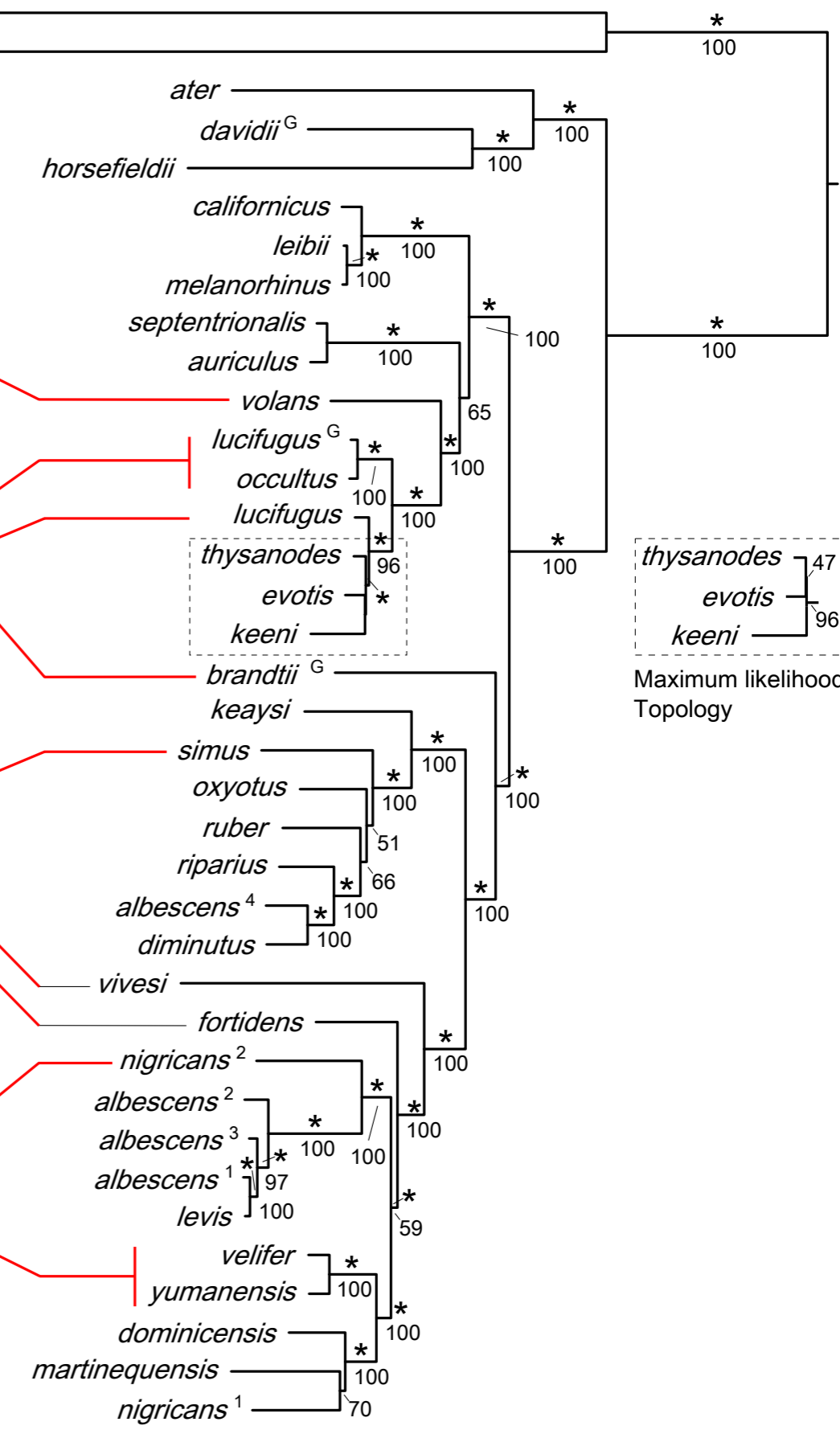


- 717 Fitch JH, Shump KA. 1979. *Myotis keenii*. Mammalian Species Archive 121:1-3.
- 718 Glenn TC, Nilsen R, Kieran TJ, Finger JW, Pierson TW, Bentley KE, Hoffberg S, Louha S, Garcia-De-Leon FJ,  
719 Angel del Rio Portilla M, et al. 2016. Adapterama I: Universal stubs and primers for thousands of dual-  
720 indexed Illumina libraries (iTru & iNext). bioRxiv.
- 721 Good JM, Vanderpool D, Keeble S, Bi K. 2015. Negligible nuclear introgression despite complete  
722 mitochondrial capture between two species of chipmunks. *Evolution* 69:1961-1972.
- 723 Gordon A, Hannon G. 2010. Fastx-toolkit. [http://hannonlab.cshl.edu/fastx\\_toolkit](http://hannonlab.cshl.edu/fastx_toolkit).
- 724 Grabherr MG, Haas BJ, Yassour M, Levin JZ, Thompson DA, Amit I, Adiconis X, Fan L, Raychowdhury R,  
725 Zeng Q, et al. 2011. Full-length transcriptome assembly from RNA-Seq data without a reference  
726 genome. *Nat Biotech* 29:644-652.
- 727 Green RE, Braun EL, Armstrong J, Earl D, Nguyen N, Hickey G, Vandewege MW, St. John JA, Capella-  
728 Gutiérrez S, Castoe TA, et al. 2014. Three crocodylian genomes reveal ancestral patterns of evolution  
729 among archosaurs. *Science* 346.
- 730 Hahn C, Bachmann L, Chevreaux B. 2013. Reconstructing mitochondrial genomes directly from genomic  
731 next-generation sequencing reads—a baiting and iterative mapping approach. *Nucleic Acids Research*  
732 41:e129.
- 733 Haynie ML, Tsuchiya MTN, Ospina-Garcés SM, Arroyo-Cabrales J, Medellín RA, Polaco OJ, Maldonado JE.  
734 2016. Placement of the rediscovered *Myotis planiceps* (Chiroptera: Vespertilionidae) within the *Myotis*  
735 phylogeny. *Journal of Mammalogy* 97:701-712.
- 736 Hedtke SM, Townsend TM, Hillis DM. 2006. Resolution of phylogenetic conflict in large data sets by  
737 increased taxon sampling. *Systematic Biology* 55:522-529.
- 738 Hollister N. 1909. Two new bats from the southwestern United States: publisher not identified.
- 739 Hosner PA, Faircloth BC, Glenn TC, Braun EL, Kimball RT. 2016. Avoiding missing data biases in  
740 phylogenomic inference: An empirical study in the landfowl (Aves: Galliformes). *Molecular Biology and*  
741 *Evolution* 33:1110-1125.
- 742 Huang H, He Q, Kubatko LS, Knowles LL. 2010. Sources of error inherent in species-tree estimation:  
743 Impact of mutational and coalescent effects on accuracy and implications for choosing among  
744 different methods. *Systematic Biology* 59:573-583.
- 745 Huang W, Zhou G, Marchand M, Ash JR, Morris D, Van Dooren P, Brown JM, Gallivan KA, Wilgenbusch  
746 JC. 2016. TreeScaper: Visualizing and extracting phylogenetic signal from sets of trees. *Molecular*  
747 *Biology and Evolution*.
- 748 Hudson RR, Coyne JA, Huelsenbeck J. 2002. Mathematical consequences of the genealogical species  
749 concept. *Evolution* 56:1557-1565.
- 750 Kapusta A, Suh A, Feschotte C. 2017. Dynamics of genome size evolution in birds and mammals.  
751 *Proceedings of the National Academy of Sciences* 114:E1460-E1469.
- 752 Katoh K, Misawa K, Kuma Ki, Miyata T. 2002. MAFFT: a novel method for rapid multiple sequence  
753 alignment based on fast Fourier transform. *Nucleic Acids Research* 30:3059-3066.
- 754 Lack JB, Roehrs ZP, Stanley CE, Ruedi M, Van Den Bussche RA. 2010. Molecular phylogenetics of *Myotis*  
755 indicate familial-level divergence for the genus *Cistugo* (Chiroptera). *Journal of Mammalogy* 91:976-  
756 992.
- 757 Lanfear R, Calcott B, Ho SYW, Guindon S. 2012. PartitionFinder: Combined selection of partitioning  
758 schemes and substitution models for phylogenetic analyses. *Molecular Biology and Evolution* 29:1695-  
759 1701.
- 760 Larsen RJ, Knapp MC, Genoways HH, Khan FAA, Larsen PA, Wilson DE, Baker RJ. 2012. Genetic diversity  
761 of neotropical *Myotis* (Chiroptera: Vespertilionidae) with an emphasis on South American species.  
762 *PLoS ONE* 7:e46578.
- 763 LaVal RK. 1973. A revision of the Neotropical bats of the genus *Myotis*: Natural History Museum, Los  
764 Angeles County.

- 765 Leaché AD, Rannala B. 2011. The accuracy of species tree estimation under simulation: A comparison of  
766 methods. *Systematic Biology* 60:126-137.
- 767 Leavitt DH, Marion AB, Hollingsworth BD, Reeder TW. 2017. Multilocus phylogeny of alligator lizards  
768 (Elgaria, Anguidae): Testing mtDNA introgression as the source of discordant molecular phylogenetic  
769 hypotheses. *Molecular Phylogenetics and Evolution*.
- 770 Lewin-Koh N. 2011. Hexagon binning: an overview.  
771 [ftp://ftp.naist.jp/pub/lang/R/CRAN/web/packages/hexbin/vignettes/hexagon\\_binning.pdf](ftp://ftp.naist.jp/pub/lang/R/CRAN/web/packages/hexbin/vignettes/hexagon_binning.pdf).
- 772 Li G, Davis BW, Eizirik E, Murphy WJ. 2016. Phylogenomic evidence for ancient hybridization in the  
773 genomes of living cats (Felidae). *Genome Research* 26:1-11.
- 774 Li H, Durbin R. 2009. Fast and accurate short read alignment with Burrows–Wheeler transform.  
775 *Bioinformatics* 25:1754-1760.
- 776 Liu L, Yu L, Kubatko L, Pearl DK, Edwards SV. 2009. Coalescent methods for estimating phylogenetic  
777 trees. *Molecular Phylogenetics and Evolution* 53:320-328.
- 778 Maddison WP, Knowles LL. 2006. Inferring phylogeny despite incomplete lineage sorting. *Systematic  
779 Biology* 55:21-30.
- 780 Manning RW, Jones JK. 1989. *Myotis evotis*. *Mammalian Species Archive* 329:1-5.
- 781 McCormack JE, Harvey MG, Faircloth BC, Crawford NG, Glenn TC, Brumfield RT. 2013. A Phylogeny of  
782 birds based on over 1,500 loci collected by target enrichment and high-throughput sequencing. *PLoS  
783 ONE* 8:e54848.
- 784 McGee MD, Faircloth BC, Borstein SR, Zheng J, Darrin Hulsey C, Wainwright PC, Alfaro ME. 2016.  
785 Replicated divergence in cichlid radiations mirrors a major vertebrate innovation. *Proceedings of the  
786 Royal Society B: Biological Sciences* 283.
- 787 Meiklejohn KA, Faircloth BC, Glenn TC, Kimball RT, Braun EL. 2016. Analysis of a rapid evolutionary  
788 radiation using Ultraconserved Elements: Evidence for a bias in some multispecies coalescent  
789 methods. *Systematic Biology* 65:612-627.
- 790 Miller Jr GS, Allen G. 1928. The American bats of the genus *Myotis* and *Pixonyx*. *Bulletin of the United  
791 States National Museum* 144:1-218.
- 792 Mirarab S, Bayzid MS, Boussau B, Warnow T. 2014. Statistical binning enables an accurate coalescent-  
793 based estimation of the avian tree. *Science* 346.
- 794 Mirarab S, Bayzid MS, Warnow T. 2016. Evaluating summary methods for multilocus species tree  
795 estimation in the presence of incomplete lineage sorting. *Systematic Biology* 65:366-380.
- 796 Mirarab S, Warnow T. 2015. ASTRAL-II: Coalescent-based species tree estimation with many hundreds of  
797 taxa and thousands of genes. *Bioinformatics* 31:i44-i52.
- 798 Morales AE, Jackson ND, Dewey TA, O’Meara BC, Carstens BC. 2016. Speciation with gene flow in North  
799 American *Myotis* bats. *Systematic Biology*.
- 800 O’Farrell MJ, Studier EH. 1980. *Myotis thysanodes*. *Mammalian Species* 137:1-5.
- 801 Pattengale ND, Alipour M, Bininda-Emonds ORP, Moret BME, Stamatakis A. 2009. How many bootstrap  
802 replicates are necessary? In: Batzoglou S, editor. *Research in Computational Molecular Biology: 13th  
803 Annual International Conference, RECOMB 2009, Tucson, AZ, USA, May 18-21, 2009. Proceedings.*  
804 Berlin, Heidelberg: Springer Berlin Heidelberg. p. 184-200.
- 805 Piaggio AJ, Valdez EW, Bogan MA, Spicer GS. 2002. Systematics of *Myotis occultus* (Chiroptera:  
806 Vespertilionidae) inferred from sequences of two mitochondrial genes. *Journal of Mammalogy* 83:386-  
807 395.
- 808 Platt RN, Vandewege MW, Kern C, Schmidt CJ, Hoffmann FG, Ray DA. 2014. Large numbers of novel  
809 miRNAs originate from DNA transposons and are coincident with a large species radiation in bats.  
810 *Molecular Biology and Evolution* 31:1536-1545.

- 811 Platt RN, Zhang Y, Witherspoon DJ, Xing J, Suh A, Keith MS, Jorde LB, Stevens RD, Ray DA. 2015. Targeted  
812 capture of phylogenetically informative Ves SINE Insertions in genus *Myotis*. *Genome Biology and*  
813 *Evolution* 7:1664-1675.
- 814 Pritham EJ, Feschotte C. 2007. Massive amplification of rolling-circle transposons in the lineage of the  
815 bat *Myotis lucifugus*. *Proceedings of the National Academy of Sciences* 104:1895-1900.
- 816 Puechmaille SJ, Allegrini B, Boston ESM, Dubourg-Savage M-J, Evin A, Knochel A, Le Bris Y, Lecoq V,  
817 Lemaire M, Rist D, et al. 2012. Genetic analyses reveal further cryptic lineages within the *Myotis*  
818 *nattereri* species complex. *Mammalian Biology* 77:224-228.
- 819 Rambaut A, Drummond A. 2013. TreeAnnotator v1. 7.0.
- 820 Rambaut A, Suchard M, Xie D, Drummond A. 2014. Tracer v1.6.
- 821 Ray DA, Feschotte C, Pagan HJT, Smith JD, Pritham EJ, Arensburger P, Atkinson PW, Craig NL. 2008.  
822 Multiple waves of recent DNA transposon activity in the bat, *Myotis lucifugus*. *Genome Research*  
823 18:717-728.
- 824 Ray DA, Pagan HJT, Thompson ML, Stevens RD. 2007. Bats with hATs: Evidence for recent DNA  
825 transposon activity in genus *Myotis*. *Molecular Biology and Evolution* 24:632-639.
- 826 Rice P, Longden I, Bleasby A. 2000. EMBOSS: the European molecular biology open software suite. In:  
827 Elsevier Current Trends.
- 828 Rodríguez-Ezpeleta N, Brinkmann H, Roure B, Lartillot N, Lang BF, Philippe H. 2007. Detecting and  
829 overcoming systematic errors in genome-scale phylogenies. *Systematic Biology* 56:389-399.
- 830 Roehrs ZP, Lack JB, Van Den Bussche RA. 2010. Tribal phylogenetic relationships within Vespertilioninae  
831 (Chiroptera: Vespertilionidae) based on mitochondrial and nuclear sequence data. *Journal of*  
832 *Mammalogy* 91:1073-1092.
- 833 Ruedi M, Mayer F. 2001. Molecular systematics of bats of the genus *Myotis* (Vespertilionidae) suggests  
834 deterministic ecomorphological convergences. *Molecular Phylogenetics and Evolution* 21:436-448.
- 835 Ruedi M, Stadelmann B, Gager Y, Douzery EJP, Francis CM, Lin L-K, Guillén-Servent A, Cibois A. 2013.  
836 Molecular phylogenetic reconstructions identify East Asia as the cradle for the evolution of the  
837 cosmopolitan genus *Myotis* (Mammalia, Chiroptera). *Molecular Phylogenetics and Evolution* 69:437-  
838 449.
- 839 Sanderson MJ, Shaffer HB. 2002. Troubleshooting molecular phylogenetic analyses. *Annual Review of*  
840 *Ecology and Systematics* 33:49-72.
- 841 Seo T-K. 2008. Calculating bootstrap probabilities of phylogeny using multilocus sequence data.  
842 *Molecular Biology and Evolution* 25:960-971.
- 843 Shimodaira H. 2002. An Approximately Unbiased test of phylogenetic tree selection. *Systematic Biology*  
844 51:492-508.
- 845 Shimodaira H, Hasegawa M. 2001. CONSEL: For assessing the confidence of phylogenetic tree selection.  
846 *Bioinformatics* 17:1246-1247.
- 847 Shimodaira H, Hasegawa M. 1999. Multiple comparisons of log-likelihoods with applications to  
848 phylogenetic inference. *Molecular Biology and Evolution* 16:1114.
- 849 Simmons NB. 2005. Order Chiroptera. *Mammal species of the world: a taxonomic and geographic*  
850 *reference* 1:312-529.
- 851 Simões BF, Rebelo H, Lopes RJ, Alves PC, Harris DJ. 2007. Patterns of genetic diversity within and  
852 between *Myotis d. daubentonii* and *M. d. nathalinae* derived from cytochrome *b* mtDNA sequence  
853 data. *Acta Chiropterologica* 9:379-389.
- 854 Sota T. (Sota2002 co-authors). 2002. Radiation and reticulation: extensive introgressive hybridization in  
855 the carabid beetles *Ohomopterus* inferred from mitochondrial gene genealogy. *Population Ecology*  
856 44:0145-0156.

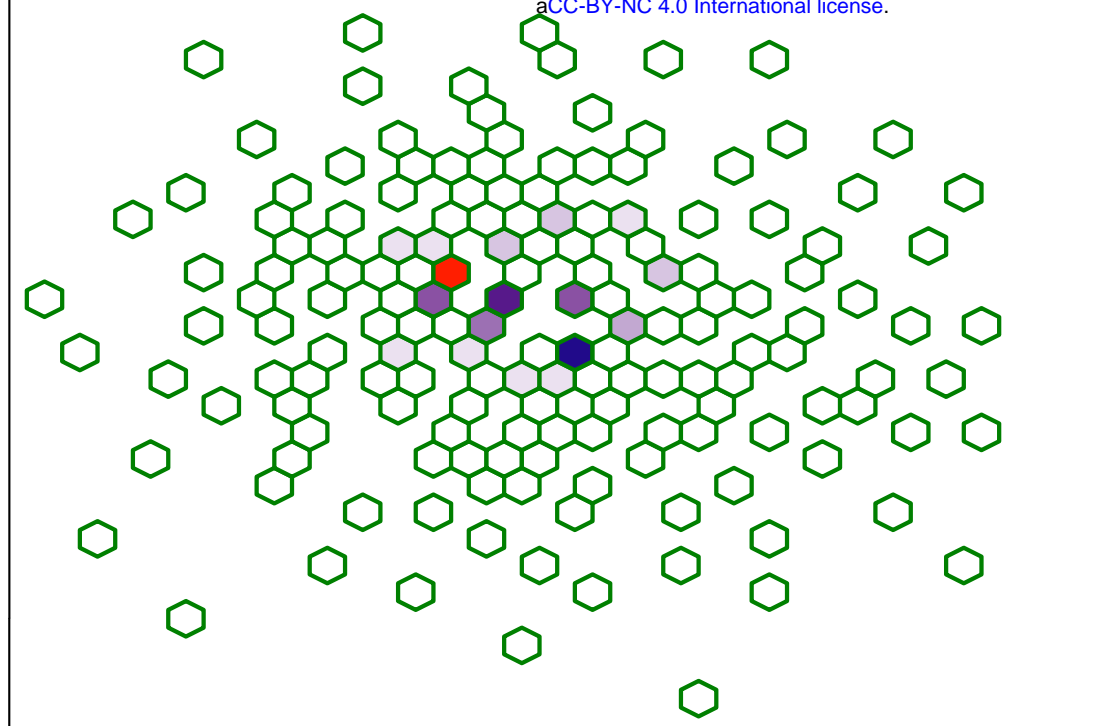
- 857 Stadelmann B, Lin LK, Kunz TH, Ruedi M. 2007. Molecular phylogeny of New World *Myotis* (Chiroptera,  
858 Vespertilionidae) inferred from mitochondrial and nuclear DNA genes. *Molecular Phylogenetics and*  
859 *Evolution* 43:32-48.
- 860 Stamatakis A. 2006. RAxML-VI-HPC: maximum likelihood-based phylogenetic analyses with thousands of  
861 taxa and mixed models. *Bioinformatics* 22:2688-2690.
- 862 Stamatakis A. 2014. RAxML version 8: A tool for phylogenetic analysis and post-analysis of large  
863 phylogenies. *Bioinformatics* 30:1312-1313.
- 864 Swofford DL. 2003. PAUP\*. Phylogenetic analysis using parsimony (\* and other methods). Version 4.
- 865 Thomas J, Sorourian M, Ray D, Baker RJ, Pritham EJ. 2011. The limited distribution of Helitrons to vesper  
866 bats supports horizontal transfer. *Gene* 474:52-58.
- 867 Vachaspati P, Warnow T. (Vachaspati2015 co-authors). 2015. ASTRID: Accurate Species TRees from  
868 Internode Distances. *BMC Genomics* 16:S3.
- 869 Valdez EW, Choate JR, Bogan MA, Yates TL. 1999. Taxonomic status of *Myotis occultus*. *Journal of*  
870 *Mammalogy* 80:545-552.
- 871 Warner RM. 1982. *Myotis auriculus*. *Mammalian Species* 191:1-3.
- 872 Wiens JJ, Kuczynski CA, Smith SA, Mulcahy DG, Sites JJW, Townsend TM, Reeder TW. 2008. Branch  
873 lengths, support, and congruence: Testing the phylogenomic approach with 20 nuclear loci in snakes.  
874 *Systematic Biology* 57:420-431.
- 875 Willis SC, Farias IP, Ortí G. 2014. Testing mitochondrial capture and deep coalescence in Amazonian  
876 cichlid fishes (Cichlidae: *Cichla*). *Evolution* 68:256-268.
- 877

**A****B**

A



bioRxiv preprint doi: <https://doi.org/10.1101/112581>; this version posted March 1, 2017. The copyright holder for this preprint (which was not certified by peer review) is the author/funder, who has granted bioRxiv a license to display the preprint in perpetuity. It is made available under aCC-BY-NC 4.0 International license.



Legend

Marker type

Nuclear UCE

Mitochondrial

Number of trees

40

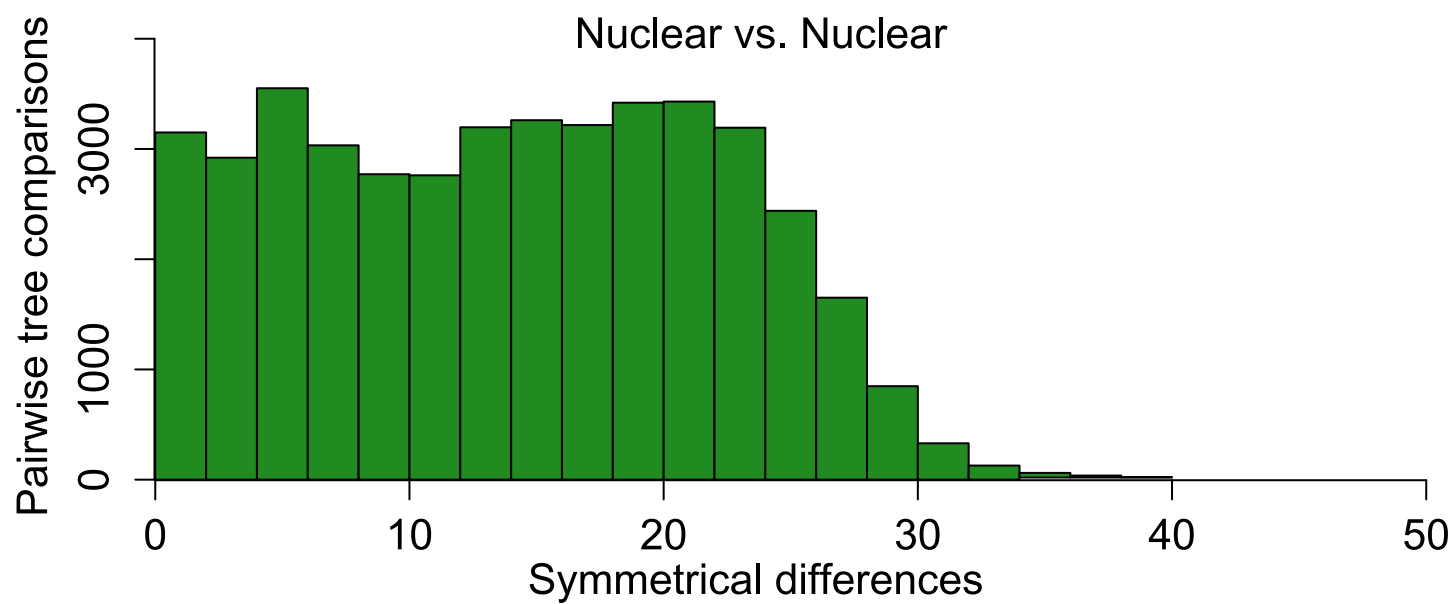
30

20

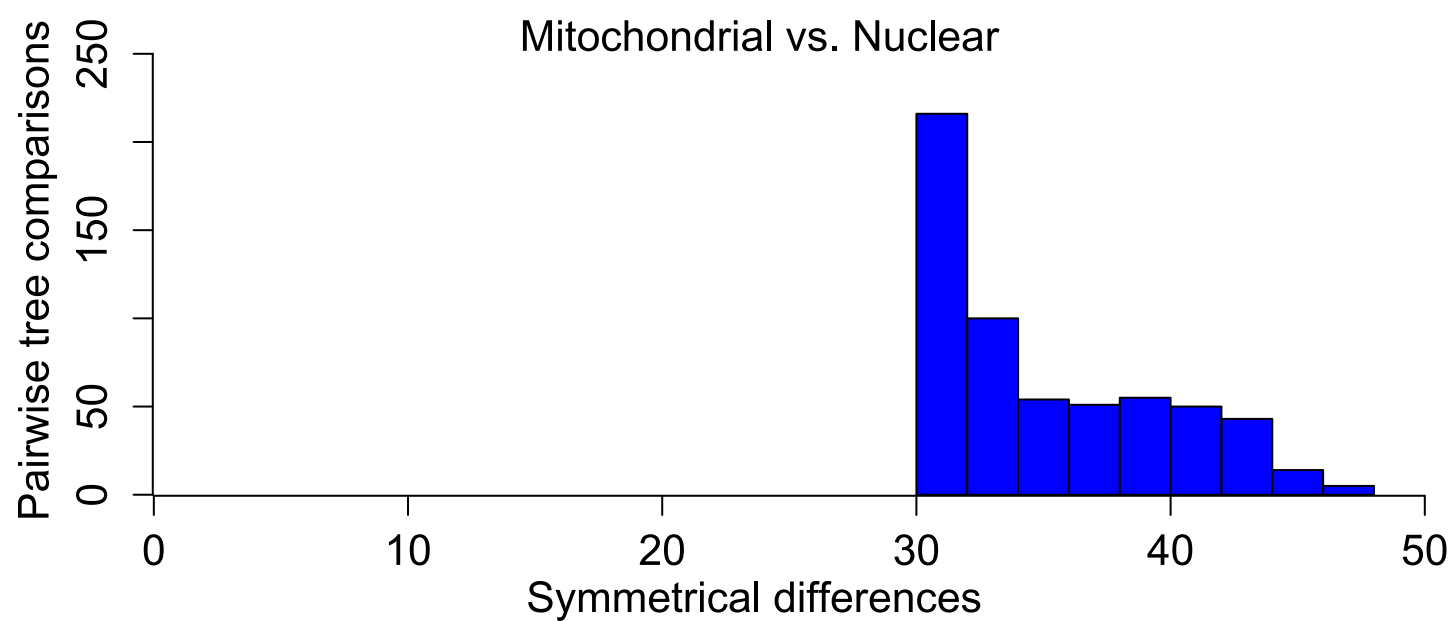
10

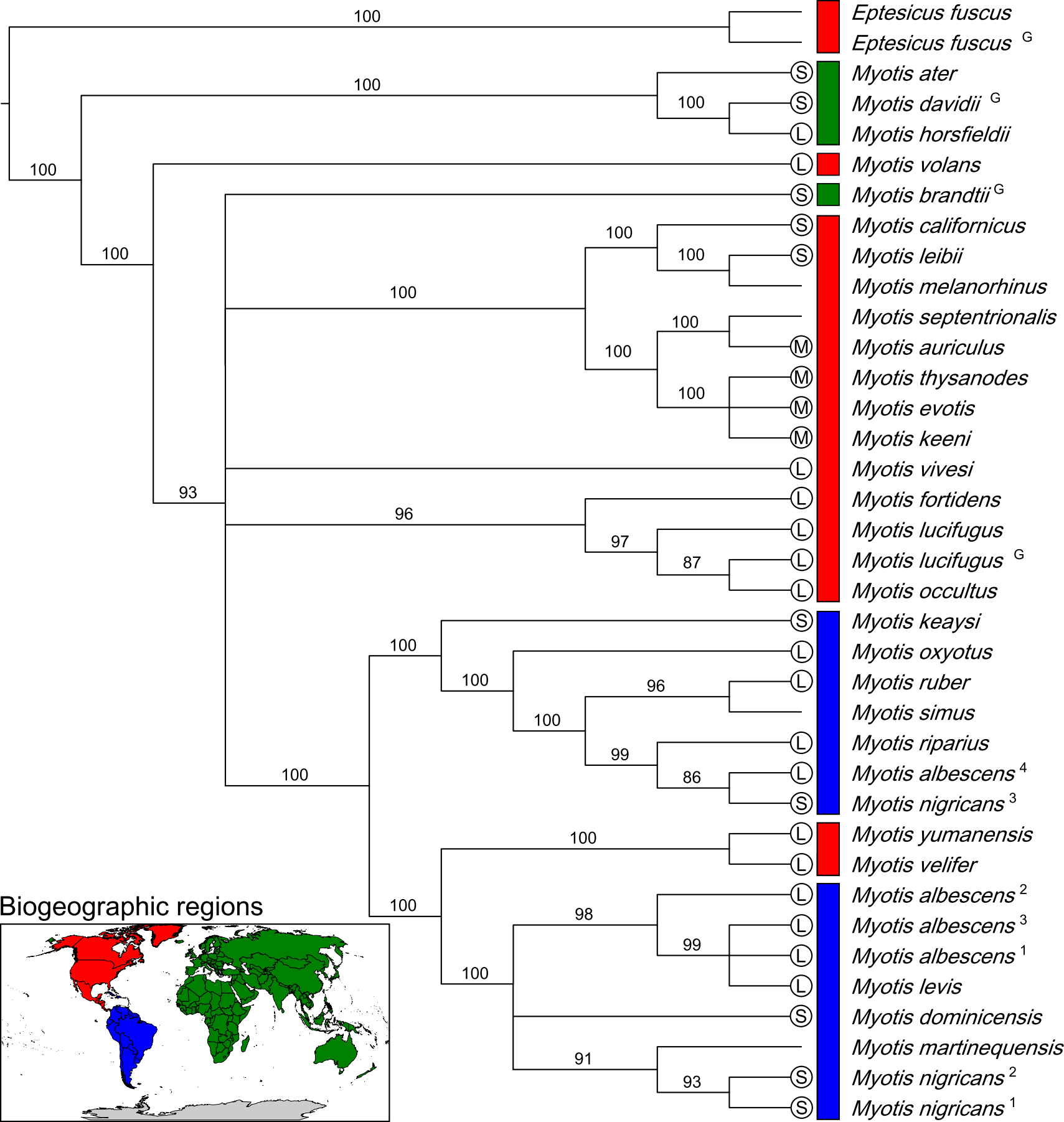
1

B



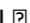
C





**Table 1 - Specimens Examined**

Genus	Specific epithet	Name herein	Museum identification num.	UCE contig Num. UCE Loci	accession	Mitochondrial genome accession
<i>Eptesicus</i>	<i>fuscus</i>	<i>fuscus</i>	TK 178736	2,849	Pending	Pending
<i>Eptesicus</i>	<i>fuscus</i>	<i>fuscus</i> <sup>G</sup>	GCA_000308155.1	2,467	Pending	Pending
<i>Myotis</i>	<i>albescens</i>	<i>albescens</i> <sup>1</sup>	RDS 7889	2,764	Pending	Pending
<i>Myotis</i>	<i>albescens</i>	<i>albescens</i> <sup>2</sup>	QCAZ 9157	1,185	Pending	Pending
<i>Myotis</i>	<i>albescens</i>	<i>albescens</i> <sup>3</sup>	TK 61766	2,872	Pending	Pending
<i>Myotis</i>	<i>albescens</i>	<i>albescens</i> <sup>4</sup>	TK 101723	2,990	Pending	Pending
<i>Myotis</i>	<i>atacamensis</i>	<i>atacamensis</i>	M4430	2,774	Pending	Pending
<i>Myotis</i>	<i>auriculus</i>	<i>auriculus</i>	MSB 40883	2,229	Pending	Pending
<i>Myotis</i>	<i>brandtii</i>	<i>brandtii</i> <sup>G</sup>	GCA_000412655.1	2,446	Pending	Pending
<i>Myotis</i>	<i>septentrionalis</i>	<i>septentrionalis</i>	RDS 7705	2,916	Pending	Pending
<i>Myotis</i>	<i>californicus</i>	<i>californicus</i>	UMMZ 175828	2,948	Pending	Pending
<i>Myotis</i>	<i>davidii</i>	<i>davidii</i> <sup>G</sup>	GCA_000327345.1	2,450	Pending	Pending
<i>Myotis</i>	<i>dominicensis</i>	<i>dominicensis</i>	TK 15624	2,576	Pending	Pending
<i>Myotis</i>	<i>evotis</i>	<i>evotis</i>	MSB 47323	2,586	Pending	Pending
<i>Myotis</i>	<i>fortidens</i>	<i>fortidens</i>	MSB 54941	2,791	Pending	Pending
<i>Myotis</i>	<i>horsfieldii</i>	<i>horsefeldii</i>	MHNG 1926.039	3,017	Pending	Pending
<i>Myotis</i>	<i>keaysi</i>	<i>keaysi</i>	TK 13525	3,195	Pending	Pending
<i>Myotis</i>	<i>keenii</i>	<i>keenii</i>	UAM 113849	2,723	Pending	Pending
<i>Myotis</i>	<i>leibii</i>	<i>leibii</i>	TK 24872	3,119	Pending	Pending
<i>Myotis</i>	<i>levis</i>	<i>levis</i>	RDS 7781	2,538	Pending	Pending
<i>Myotis</i>	<i>lucifugus</i>	<i>lucifugus</i>	MSB 46679	2,736	Pending	Pending
<i>Myotis</i>	<i>lucifugus</i>	<i>lucifugus</i> <sup>G</sup>	GCA_000147115.1	2,429	Pending	Pending
<i>Myotis</i>	<i>martiniquensis</i>	<i>martiniquensis</i>	TK 151413	856	Pending	Pending
<i>Myotis</i>	<i>melanorhinus</i>	<i>melanorhinus</i>	M8944	3,177	Pending	Pending
<i>Myotis</i>	<i>nigricans</i>	<i>nigricans</i> <sup>1</sup>	QCAZ 9601	2,854	Pending	Pending
<i>Myotis</i>	<i>nigricans</i>	<i>nigricans</i> <sup>2</sup>	RDS 7791	3,159	Pending	Pending
<i>Myotis</i>	<i>nigricans</i> or <i>diminutus</i>	<i>nigricans</i> <sup>3</sup>	QCAZ 9168	3,078	Pending	Pending
<i>Myotis</i>	<i>occultus</i>	<i>occultus</i>	MSB 121995	2,957	Pending	Pending
<i>Myotis</i>	<i>oxyotus</i>	<i>oxyotus</i>	UMMZ RCO1013	3,106	Pending	Pending
<i>Myotis</i>	<i>riparius</i>	<i>riparius</i>	TK 145199	2,890	Pending	Pending
<i>Myotis</i>	<i>ruber</i>	<i>ruber</i>	MVZ 185692	2,757	Pending	Pending
<i>Myotis</i>	<i>simus</i>	<i>simus</i>	TK 22688	2,924	Pending	Pending
<i>Myotis</i>	<i>thysanodes</i>	<i>thysanodes</i>	07LEP	2,821	Pending	Pending
<i>Myotis</i>	<i>velifer</i>	<i>velifer</i>	MSB 70877	2,704	Pending	Pending
<i>Myotis</i>	<i>vivesi</i>	<i>vivesi</i>	MSB 42658	2,469	Pending	Pending
<i>Myotis</i>	<i>volans</i>	<i>volans</i>	MSB 40886	2,819	Pending	Pending
<i>Myotis</i>	<i>yumanensis</i>	<i>yumanensis</i>	RDS 7734	2,589	Pending	Pending

Collection abbreviations: Museum of Southwestern Biology (MSB), Museum of Vertebrate Zoology (MVZ), Natural History Museum of Geneva (MHNG), Pontificia Universidad Catolica del Ecuador Museo de Zoologia (QCAZ), Texas Tech University Natural Science Research Laboratory (TK), University of Alaska Museum of the North (UAM), University of Michigan Museum of Zoology (UMMZ). Samples beginning with "GCA\_" represent genome assemblies available through NCBI. 



**Table 2. Character information**

<b>Min. num. of taxa</b>	<b>Percent of taxa per locus</b>	<b>Number of Loci</b>	<b>Parsimony-informative characters</b>	<b>Variable uninformative</b>	<b>Alignment length</b>	<b>Optimum Partitions</b>
37	100	212	3,480	4,778	112,125	6
35	95	1,193	18,288	24,189	575,321	15
31	85	2,034	29,179	41,711	903,903	16
27	75	2,481	33,031	48,732	1,041,099	20
24	65	2,668	34,373	51,148	1,091,620	27
20	55	2,890	35,284	53,200	1,144,471	27
16	45	3,064	36,539	54,782	1,187,492	31
12	35	3,232	37,259	56,453	1,227,093	34
9	25	3,379	37,894	57,672	1,260,248	37
5	15	3,648	38,718	62,588	1,377,262	31

General alignment information. For a subset of analyses a series of alignments were generated based on the number of taxa per locus. Thirty-seven taxa were examined so an alignment with all 37 taxa was considered 100% complete. Parsimony-informative characters make up a small portion of the total alignment. The optimum partitioning scheme was calculated with PartitionFinder.